PECTUS BAR BENDER AND DESIGNER SOFTWARE TO ENHANCE PECTUS EXCAVATUM SURGERIES

by

Kenan Kaan Kurt

B.S., in Control and Automation Engineering, Istanbul Technical University, 2017

Submitted to the Institute of Biomedical Engineering
in partial fulfillment of the requirements
for the degree of
Master of Science
in
Biomedical Engineering

Boğaziçi University
2020

PECTUS BAR BENDER AND DESIGNER SOFTWARE TO ENHANCE PECTUS EXCAVATUM SURGERIES

APPROVED BY:

Assoc. Prof. Özgür Kocatürk .....
(Thesis Advisor)

Prof. Can Yücesoy .....

Prof. İnci Çilesiz .....

DATE OF APPROVAL: 30 JANUARY 2020

ACKNOWLEDGMENTS

I would like to express my sincerest respect to my thesis advisor Assoc. Prof. Dr. Özgür Kocatürk for guiding me through this process. In addition, I would like to thank Associate Professor Erkan Yıldırım for his contributions and his experienced perspective.

Additionally, I would also like to thank my dear wife, Büşra Bayat Kurt, for showing me patience and understanding, Hüseyin Tanzer Atay and Mustafa Alpkan Çiçek for helping me without getting tired of it, and Barış Karaca and Dr. Serkan Türkeli for their efforts.

ACADEMIC ETHICS AND INTEGRITY STATEMENT

I, Kenan Kaan Kurt, hereby certify that I am aware of the Academic Ethics and Integrity Policy issued by the Council of Higher Education (YÖK) and I fully acknowledge all the consequences due to its violation by plagiarism or any other way.

Name :

Signature:

Date:

ABSTRACT

PECTUS BAR BENDER AND DESIGNER SOFTWARE TO ENHANCE PECTUS EXCAVATUM SURGERIES

Pectus excavatum is caused by inward collapse of the rib cage, which may cause the patient's internal organs to become flush and fail to function. In 1986, Donald Nuss developed the most common treatment method today, also known as the Nuss technique. The Nuss technique is performed by opening incisions from each side of the patient's rib cage and placing a bent bar under the cage as required by the rib cage. It is still made with the help of machines that can be compared to simple hand tools. For this reason, it is difficult to adjust the bar according to the patient and usually more than one attempt is made to find the correct shape. In this process, the submerged rib cage is especially likely to come into contact with vital organs such as the heart and lung. Since the pericardium sticked to the sternum, it has to be torn in some surgeries, where the bar is in direct contact with the heart. For all these reasons, it is very important to place this bar in the patient's rib cage with least trials. In order to reduce the problems seen during the treatment phase, a web-based software using medical images is built to shape the drawn bar along with a bending machine. This allows the bender to bend the bar correctly using DICOM images of the patient before surgery, and any errors that may occur can be corrected beforehand. In addition, it is expected that the machine will shorten the operation time, reduce the number of life-threatening situations and improve the patient's quality of life. The system bends bars with an error rate under 8% at any given point on the bar, which is sufficient according to consultant surgeon. Also, the bending process is completed under 1 minute with the help of 28 Nm stepper motor.

Keywords: Pectus excavatum, bender, designer.

ÖZET

PECTUS EXCAVATUM TEDAVİSİ İÇİN BAR BÜKÜCÜ VE TASARIM YAZILIMININ TASARLANMASI

Pectus excavatum göğüs kafesinin içeri doğru çökmesi ile oluşur bu sebeple hastanın iç organlarının şıkışmasına ve işlevlerini yerine getirememesine sebebiyet verebilir. 1986 yılında Donald Nuss Nuss tekniği olarak da bilinen günümüzdeki en yaygın tedavi yöntemini geliştirmiştir. Nuss tekniği hastanın göğüs kafesinin 2 yanından kesiler açılması ve göğüs kafesinin alması gereken şekilde bükülen bir barın kafes altına yerleştirilmesi ile gerçekleştirilmektedir. Bu tedavi şeklinde bar şekillendirme halen basit el aletlerine benzetilebilecek makineler yardımıyla yapılmaktadır. Bu sebepten dolayı barın hastaya göre ayarlanması güç olmakta ve doğru şeklin bulunabilmesi için birden fazla deneme yapılmaktadır. Bu süreçte batmış olan göğüs kafesinin özellikle kalp ve akciğer gibi hayati organlara temas etme olasılığı vardır. Bazı ameliyatlarda sternuma yapışan perikardiyum yırtılmak zorunda kaldığından barın kalbe direkt teması söz konusudur. Bütün bu sebeplerden dolayı bu barın en az denemede hastanın göğüs kafesine yerleştirilmesi çok önemlidir. Tedavi aşamasında görülen sorunların azaltılması adına hastanın medikal görüntüleri kullanarak web tabanlı bir yazılım vasıtasıyla bar çizimi yapılmasını ve çizilen barın tasarlanan bükücü makine yardımıyla şekillendirilmesi sağlanmıştır. Bu sayede bükücü ameliyattan önce hastanın DICOM görüntülerini kullanarak barı doğru bir şekilde bükebilir ve oluşabilecek hatalar önceden düzeltilebilir. Ek olarak, makinenin ameliyat süresini kısaltması, oluşabilecek hayati tehlikeleri azaltılması ve hastanın yaşam kalitesini artırması beklenmektedir. Sistem herhangi bir noktada %8'den daha az hata oranıyla büküm işlemini gerçekleştirmektedir. Bu oran danışman cerrah tarafından yeterli görülmüştür. Ayrıca bütün büküm işlemi 28Nm tork üretebilen step motor vasıtasıyla 1 dakikanın altında gerçekleştirilmektedir.

Anahtar Sözcükler: Pektus ekskavatum, bar bükcü, tasarım aracı.

TABLE OF CONTENTS

ACKNOWLEDGMENTS . . . iii
ACADEMIC ETHICS AND INTEGRITY STATEMENT . . . iv
ABSTRACT . . . v
ÖZET . . . vi
LIST OF FIGURES . . . ix
LIST OF TABLES . . . xi
LIST OF SYMBOLS . . . xii
LIST OF ABBREVIATIONS . . . xiii
1. INTRODUCTION . . . 1
1.1 Statement of Problem . . . 1
1.2 Objective . . . 3
2. BACKGROUND . . . 4
2.1 Anatomy of Chest . . . 4
2.2 Pectus Excavatum . . . 5
2.2.1 General Information . . . 5
2.2.2 History & Therapeutic Procedures . . . 7
2.2.3 Symptoms & Commonness . . . 10
2.2.4 Preoperative Procedure & Evaluation Criteria . . . 11
2.3 DICOM . . . 15
3. METHOD . . . 16
3.1 Requirements and Specifications . . . 16
3.2 Mechanical Design . . . 19
3.2.1 Automated Bar Bender Design . . . 19
3.2.2 Bender Head Design . . . 21
3.2.3 Motor Holder Design . . . 22
3.2.4 Linear Timing Belt Module . . . 23
3.2.4.1 General Specifications . . . 23
3.2.4.2 Technical Specifications . . . 24
3.2.4.3 Loading Capacity . . . 25

3.3 Electrical Design . . . 26
3.3.1 Microprocessor . . . 26
3.3.2 Motor Specifications . . . 27
3.3.3 Motor Drivers . . . 29
3.3.3.1 CW2283 Motor Driver . . . 29
3.3.3.2 CWD556-A Motor Driver . . . 30
3.4 Software Design . . . 32
3.4.1 Back-end . . . 32
3.4.1.1 Programming Language Selection . . . 32
3.4.1.2 Integration DICOM with NodeJs . . . 32
3.4.2 Front-end . . . 33
3.4.2.1 Framework Selection . . . 33
3.4.2.2 Components . . . 33
3.4.2.3 Forming Transverse and Sagittal Images . . . 34
3.4.2.4 Drawing Bèzier Curves . . . 34
3.4.2.5 Sampling Data Points . . . 36
3.4.2.6 Pixel to Actual Length Calculation . . . 37
3.4.2.7 Graphical User Interface Design . . . 37
3.4.3 Embedded Software . . . 42
3.4.3.1 Programming Language Selection . . . 42
3.5 Bar Bending Process . . . 42
4. RESULTS . . . 44
4.1 Statement of Results . . . 44
5. CONCLUSION AND FUTURE WORKS . . . 50
5.1 Conclusions . . . 50
5.2 Statement of Existing Problems . . . 51
5.3 Limitations . . . 52
5.4 Future Works . . . 53
REFERENCES . . . 54

LIST OF FIGURES

Figure 1.1	Different models of the vacuum bell.	1
Figure 1.2	A pectus bar.	2
Figure 1.3	A variety of pectus bar benders used in surgeries.	2
Figure 2.1	The thoracic wall.	4
Figure 2.2	The welch index.	12
Figure 2.3	The symmetry index measurement over the thorax CT.	13
Figure 2.4	The angle of sternal torsion.	14
Figure 3.1	Biodesign innovation process.	16
Figure 3.2	The outline view of the chassis.	19
Figure 3.3	The side view of the chassis.	20
Figure 3.4	The zoomed view of the chassis.	20
Figure 3.5	The first design of 6 holes bender head. (a.Top view b.Bottom view)	21
Figure 3.6	The technical drawing of the bender head.	22
Figure 3.7	Technical drawings of the motor holder.	23
Figure 3.8	The view of linear timing belt module.	24
Figure 3.9	The technical drawing of linear timing belt module.	25
Figure 3.10	The load capacity values of linear timing belt module.	25
Figure 3.11	ESP8266 PCB layout.	26
Figure 3.12	The module schematics of ESP8266.	27
Figure 3.13	The wiring connection diagram of the motor.	28
Figure 3.14	The motor dimensions.	28
Figure 3.15	The CW2283 motor driver.	29
Figure 3.16	The connection diagram of CW2283 motor driver.	30
Figure 3.17	The connection diagram of CWD556-A motor driver.	31
Figure 3.18	The example sagittal view of a CT image.	34
Figure 3.19	The example transverse view of a CT image.	35
Figure 3.20	Various Bèzier curves with different control points.	36
Figure 3.21	The example of pixel spacing value.	37

Figure 3.22	The homepage view of the GUI.	38
Figure 3.23	The designer view of the GUI.	39
Figure 3.24	The patient information screen.	40
Figure 3.25	The toolbox of the GUI.	40
Figure 3.26	The curve drawing area of the GUI.	40
Figure 3.27	The bender setup screen of the GUI.	41
Figure 3.28	The process of bending: Points 1 through 5 shows the bending steps from a line to a curve.	43
Figure 4.1	The final prototype of the designed system.	45
Figure 4.2	The real time bending procedure with designed system by GUI.	45
Figure 4.3	The graphs of drawn and bent bar coordinates.	47
Figure 4.4	The bending procedure of bar drawn by the consultant surgeon.	48
Figure 4.5	The graphs of drawn and bent bar coordinates based on real case data.	49

LIST OF TABLES

Table 3.1	Technical specifications of the linear timing belt module.	24
Table 3.2	The specifications of 110HS28.	28
Table 3.3	The electrical specifications of the CW2283.	29
Table 3.4	The electrical specifications of the CWD556-A.	31
Table 4.1	Test results of bending procedure based on test sample.	46
Table 4.2	Test results of bending procedure based on real patient data.	48
Table 5.1	Limit values of the manufactured prototype.	52

LIST OF SYMBOLS

A	Ampere
amp	Ampere
cm	centimeter
mH	miliHenry
mm	milimeter
N	Newton
Nm	Newton*meter
steps/rev	steps/revolution
V	Volt

LIST OF ABBREVIATIONS

3D	3 Dimension
AC	Alternating Current
CNC	Computer Numerical Control
CT	Computed Tomography
DC	Direct Current
DICOM	Digital Imaging and Communications in Medicine
DSP	Digital Signal Processing
ECG	Electrocardiography
ECHO	Echocardiogram
EXIF	Exchangeable image file format
GUI	Graphical User Interface
HTML	HyperText Markup Language
IgE	Immunoglobulin E
IOT	Internet of things
JPEG	Joint photographic experts group
MVP	Mitral Valve Prolapse
NEMA	National Electrical Manufacturers Association
PCB	Printed Circuit Board
PNG	Portable Network Graphics
PTFE	polytetrafluoroethylene
PWM	Pulse Width Modulation
SDK	Software Development Kit
SRAM	Static Random Access Memory
TTCK	Medical Devices Agency of Turkey
UNSPSC	United Nations Standard Products and Services Code
WiFi	Wireless Field

1. INTRODUCTION

1.1 Statement of Problem

Pectus excavatum is a disorder due to abnormal growth of the sternum or rib cage. The rib cages of individuals with this disorder take an inward concave shape. The most common treatment options are Nuss technique, vacuum chamber technique and surgical intervention. Among these widespread options, Nuss technique is the most commonly used method [1]. Figure 1.1 shows the vacuum chamber. This device is intended for treatment by placing the patient chest and vacuuming the relevant rib cage area. However, according to the information obtained from the consultant surgeon, this device is recommended for patients with low levels of depression and should be used for at least 3-4 years for 18 hours per day.

Figure 1.1 Different models of the vacuum bell [2].

Nuss technique is an advanced and long term treatment method. Most patients with pectus excavatum can recover from their illnesses by Nuss technique. However, the complications that may occur during the operation disturb the surgeon and the patient. Although high technology is frequently used in other surgical fields, pectus excavatum

surgery is not one of them. Production of 3D printers in this area contributes, but this development rate is not yet sufficient. Therefore, it is necessary to carry out studies to improve the present treatment method. The biggest problem with the present method is that the bar is manually shaped by the surgeon (the bar is shown in Figure 1.2). The surgeon shapes the bar with the help of a material similar to a pair of iron scissors with the measurement taken from the patient (Figure 1.3). It is difficult to bend the stainless steel bars to reach the correct geometry. In some cases, the posture of the bar attached to the patient is removed and reshaped and placed in the patient. When this procedure is performed repeatedly according to the patient's condition, the operation time of the patient is prolonged, and the possibility of complications due to placement or removal increases. Increasing potential danger and being in operation increases the patient's vital risks.

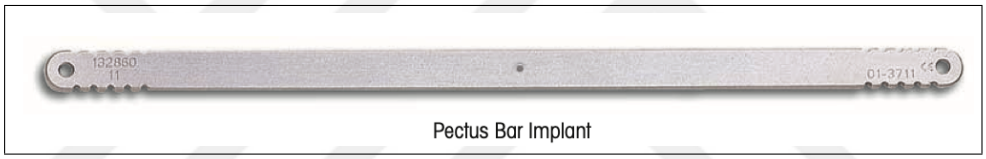

Figure 1.2 A pectus bar [3].

Figure 1.3 A variety of pectus bar benders used in surgeries [3].

1.2 Objective

Pectus excavatum is a deformity that negatively affects human life and affects the functions of internal organs. Correction of deformities is important since the rib cage maintains and contains structures that are important for the functions of the body, such as the lung, heart, esophagus, trachea, diaphragm, and main vessels of the heart.

Although the Nuss technique, which is widely used, is very successful, the insufficiency of the tools used during the operation decreases the success of the surgery and reduces its effectiveness.

Within the scope of this thesis, it is aimed to develop a cost-effective pectus bar bender with high availability materials and a web-based software that can work in cloud systems that will enhance the bending process of the bar used in pectus excavatum surgeries with facilitated, and a holistic solution to improve the quality of life of the patient by preventing account and human errors.

2. BACKGROUND

2.1 Anatomy of Chest

In humans and other mammals, the area between the neck and abdomen is called thorax or chest. The thorax consists of two main parts: the thoracic cavity and the thoracic wall. The thoracic cavity contains the internal organs of the chest and is the second largest body cavity in human body. It is surrounded by a rib cage. The rib cage is surrounded by the spine and shoulder girdle. The thorax wall containing the upper bone portion of the body resembles an irregularly shaped cylinder with two narrow openings above and a large wide opening (in Figure 2.1) [4].

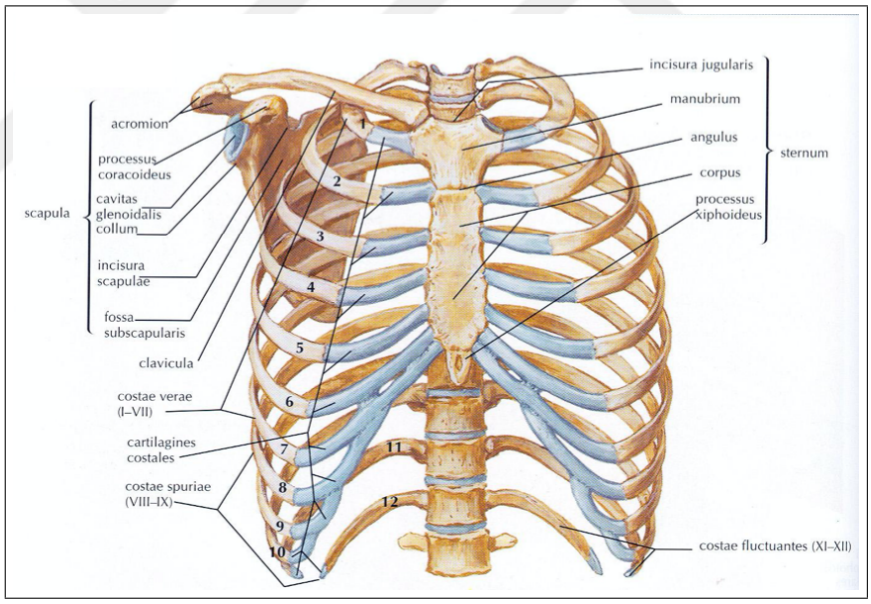

Figure 2.1 The thoracic wall, adapted from [5].

The skeleton of the thoracic wall consists of 12 thoracic vertebrae, 12 pairs of ribs, cartilage of these ribs and sternum. The posterior part of the thoracic wall consists of 12 thoracic vertebrae and discus intervertebralis between these vertebrae. The lateral sections of the thorax wall consist of 12 pairs of ribs, flat muscles of three layers covering the interstitial space between the cartilages of these ribs and adjacent ribs. The sternum forms the anterior part of the thoracic wall [6].

The cavity surrounded by the thorax wall is called the thoracic cavity (cavitas thoracis). The structures within the mediastinum and the lungs are located within the thoracic cavity. The mediastinum includes the heart, cavum pericardia, thymus, trachea, oesophagus, aorta, vena cava cranialis and other neurovascular structures. There is negative pressure in the thoracic cavity. The thoracic cavity of the mammals is covered with a thin serous membrane called the pleura. This membrane is generally called visceral pleura (pleura visceralis) if it covers the lungs and parietal pleura (pleura parietalis) if it covers the chest cavity. The large organ located in the middle of the thoracic cavity (mediastinum medium) is the heart. On the right side of the heart is the right lung. Thoracic cage is covered with skin, fascia and muscles. Some muscles here connect the shoulder girdle to the upper extremity and the trunk. In addition to protecting the thorax organs, the thoracic wall functions mechanically in respiration [6].

In addition, the thoracic cavity includes the esophagus, the channel through which food passes from the throat to the stomach. Distortions and deformations in the thoracic wall can cause significant health problems as they contain a large number of vital organs.

2.2 Pectus Excavatum

2.2.1 General Information

Pectus Excavatum is translated to Latin as "collapsed breast". Other names; "Shoemaker's chest", "trichterbrust" (funnel chest, funnel chest), "koilosternia", "chonechondrosternon" [7].

The pectus excavatum is a chest wall deformity characterized by the posterior depression of the midline and lower part of the sternum and the posterior curvature of the cartilages of the associated ribs that is translated from Latin as "collapsed breast" [7],[8]. It is also known with other names; "Shoemaker's chest", "trichterbrust" (funnel

chest), "koilosternia" and "chone-chondrosternon" [7]. When the sternum corpus is depressed with costal cartilages showing abnormal growth, the ribs protrude from the sternum to the anterior form to form this image.

In the case of deformity, the manubrium, first and second ribs are usually normal, but the depth and shape of the depression are variable.

According to morphological appearance, Kuhn et al. Divided the pectus excavatum deformities into four types [9]:

1. Localized Deep Collapse (Cup Shaped)
2. Diffuse Shallow Depression (Saucer Shaped)
3. Asymmetric Long Tubular Collapse (Grand Canyon)
4. Horseshoe Deformity (Currarino-Silverman, Horns of steer)

Pectus excavatum is the most common congenital deformity of the chest wall characterized by depression of the sternum. Although this deformity appears to affect the anterior region of the chest, it is actually a deformity associated with the entire thorax and spine. The most common musculoskeletal anomaly associated with the pectus excavatum is scoliosis with three-dimensional deformity including lateral flexion, axial rotation and flattening components of sagittal physiological curve.

Correction of pectus excavatum deformity has become widespread with the development of Nuss procedure, which is a minimally invasive operation. Nuss operation in a pectus excavatum patient may improve the concavity of the anterior thoracic region and may also have dynamic effects on the spine due to the integration of the anterior and posterior thorax.

The causes of this deformity is not known. It is most commonly seen as idiopathic. However, studies that include theories such as intrauterine pressure, ricketsets,

diaphragm anomalies have been published related to etiology [10].

In 1954, Chin et al. made diaphragm biopsies, believing that deformity was due to abnormal diaphragm, but the microscopic results of macroscopically relatively thin diaphragms were reported to be normal [11]. Lester and previous investigators have suggested that the pectus excavatum deformity is due to the short end of the central tendon of the diaphragm pulling the lower end of the sternum towards the posterior [12].

In 1967, Kenneth et al., osteogenesis and chondrogenesis failure with the formation of soft ribs and cartilage with the formation of deformity as a result of inability to resist the differential pressure [13].

In 1981, Hecker et al. defined histopathological changes in costal cartilages and reported familial predisposition in patients with pectus excavatum [14]. On the other hand, Kelly and colleagues in 2005 between the years 1889-2001 autopsy of 62 cadavers with pectus excavatum histological pathology in cartilages, but emphasized that the pectus excavatum is associated with many connective tissue diseases [15]. Serafin et al. published in 2003, although the etiology of thoracic wall deformities have not been clarified, it is noted that the failure of endochondrial ossification and growth of costal cartilages is more effective than diaphragmatic developmental defect in the formation of this deformity [16].

Shamberger et al. Reported that 37% of patients had a family history of chest wall deformity [17]. In 2009, Gurnett et al. reported in their genetic studies that the risk of pectus excavatum increased among relatives with 18th chromosome q arm [18].

2.2.2 History & Therapeutic Procedures

The available data show that the definition and clinic of pectus excavatum from the 16th century to the 20th century was examined through case reports. For the first

time in 1594, Bauhinus reported the first case by describing the clinical features of the pectus excavatum, and the study of pectus excavatum by Johan Schenck summed up the definition of pectus excavatum [19]. In 1820, Coulson published an article on the genetic predisposition to deformity [20]. The term "trichterbrust" (funnel chest) was first used in 1882 by Wilheim Ebstein in a case report [21].

The first intervention for pectus was at trial level and in 1911 Meyer excised the 2nd and 3rd costal cartilages in a pectus case but could not achieve clinical improvement [22]. Sauerbruch opened a new door in thoracic surgery by creating a negative pressure chamber in 1913 and applied bilateral costal cartilage resection and sternal osteotomy for the first time in a patient with pectus excavatum and provided regression of symptoms in the case [23].

In 1939, Ochsner and De Bakey underwent bilateral costochondral resection and transverse sternotomy; In 1944, Nissen reported that the complaints of pectus excavatum patients were improved by performing sternum and cartilage resection by reversing the sternum (sternal turnover) [24],[25]. Ravitch, who underwent bilateral cartilage resection and sternal osteotomy without external traction using a more radical modification of the Sauerbruch technique in 1947, followed frequent recurrence in this procedure.

In 1949, Ravitch and Chin reported more aggressive sternum mobilization, costal cartilage excision, and sternal fixation using Kirschner wire [11],[26]. In 1956, Wallgreen and Irrigation used a slightly inclined stainless steel rod as an internal support under the sternum [27]. Adkins and Blade 1961 described the application of steel bars behind the sternum in pectus operations [28]. Surgical correction method of pectus deformities has been formed and advanced through this technique.

In 1974, Welch and Kearney reported the incidence of the association of Prune-Belly syndrome and pectus excavatum, and Welch developed the currently valid Welch index to determine the degree of deformity [29],[30]. In 1986, Nuss developed an alternative technique for correcting the deformity without excising the ribs based on

the flexibility of costal cartilages, and developed the so-called Nuss procedure, where blood loss was minimal without rib or sternum resection. In the report of its 10-year experience, short operation time, good cosmetic results and minimal blood loss results were emphasized [31]. In 1988, Scherer pointed out the association of Marfan syndrome and accompanying scoliosis, while in 1989 Waters reported a 26% association of pectus excavatum with scoliosis [32],[33].

A study on the use of titanium plates for correction of pectus excavatum was published by Saxena et al. in 1998 [34]. Osawa et al. recommended the use of titanium bars instead of metal bars for the Nuss technique [35]. Robicsek described the modified Ravitch technique in 2000 by reducing the number of resected cartilages [36]. In a series of 303 patients published by Croitoru et al. In 2002, they stated that the best option for surgical treatment of pectus excavatum was minimally invasive Nuss technique and they reduced the complications with modifications [37].

In 2005, Schaarschmidt et al. reported in a case that bilateral thoracoscopy-assisted bar placement with extrapleural submuscular technique reduces complications such as pain, pneumothorax, bar adhesion, and pericardial effusion [38]. In the same year, Schier et al. suggested that pectus excavatum cases could be corrected by vacuum [39]. Along with the advances in surgical techniques and advances in the field of anesthesia and algology, the success rate in pectus excavatum cases has increased. In 2006, Futagawa et al. noted that epidural fentanyl infusion provides effective pain control in the postoperative period and thus prevents complications such as bar malrotation [40]. In 2008, Nuss published a series of 947 cases with satisfactory results of the Nuss procedure [41]. In 2009, Gurnett et al. reported in their genetic studies that the risk of pectus excavatum increased among relatives with the 18th chromosome q arm [18].

Recently, it has been discussed whether this chest deformity can be corrected by applying external pressure such as vacuum or magnet without the need for surgical procedure [42]. However, further experimental and clinical studies are needed on this subject.

Minimally invasive pectus repair (Nuss procedure) and open surgical methods have been compared in many studies all over the world.

2.2.3 Symptoms & Commonness

The pectus excavatum clinic covers a wide spectrum from a cosmetic problem and psychological damage to a major physiological disease such as cardiopulmonary involvement.

The majority of the cases are noticed in the first year of life, they are more asymptomatic until puberty and thus are tolerable, but with the acceleration of development during puberty, deformity becomes more prominent.

The association of skeletal muscle system anomalies associated with pectus excavatum is 18%, and the most common association is scoliosis with 15% [43]. In addition, congenital heart diseases such as asthma with 5.2% and mitral valve prolapse in 2% may accompany [44].

According to a multicenter prospective study, the most common symptom was dyspnea on exercise in 66% of patients, while the other symptoms were; limited exercise tolerance (64.5%), shortness of breath at rest (62.1%), chest pain with exercise (51.1%), chest pain not associated with exercise (32%), palpitations (11%) [45] .

Pectus excavatum is the most common congenital chest deformity in children [8]. According to the studies, it is reported that the frequency is between 1 and 300 live births, with a frequency ranging from 1 in 300 and 3 times more in boys than in girls [46]. It has been reported that the prevalence in the general population varies between 0.1% and 0.4% [47].

2.2.4 Preoperative Procedure & Evaluation Criteria

Preoperative anterior and lateral chest radiographs, thoracic CT, pulmonary function test, ECG, ECHO, blood tests levels should be evaluated for the patients who are candidates for the operation.

Chest X-rays are both necessary for preoperative anesthesia examination and scoliosis can be seen on the radiographs.

The proximity of the sternum to the vertebral column can be measured on the lateral chest X-ray, and the Welch index value, a parameter used to determine the degree of deformity, can be found. The ratio of the distance (D1) that starts from the anterior face of the 3rd thoracic vertebra and reached the posterior side of the sternum (D1) gives the ratio of sternum depression to the distance (D2) that starts from the spinos process of the 9th thoracal vertebra and is reached to the posterior side of the sternum (shown in Figure 2.2). Deformity degree formula is given in Eq. 2.1.

$$Deformity\,degree = (1 - Deformity\,ratio) * 10 \tag{2.1}$$

A scale of 1 to 10 is defined in the Welch index and progressive deformities above 5 require surgical intervention [49].

Thoracic CT informs the surgeon about the location of the intra-thoracic organs according to the effect of deformity and the thoracic skeletal system. Because, in minimally invasive surgery, knowing the location of intrathoracic organs is very useful in terms of the equipment to be used and the planning of the surgical area. Thorax CT also allows Haller index measurement to determine the degree of deformity. The Haller Index is calculated by dividing the transverse diameter of the chest at the deepest point of the sternum by the distance between the posterior side and the anterior surface of

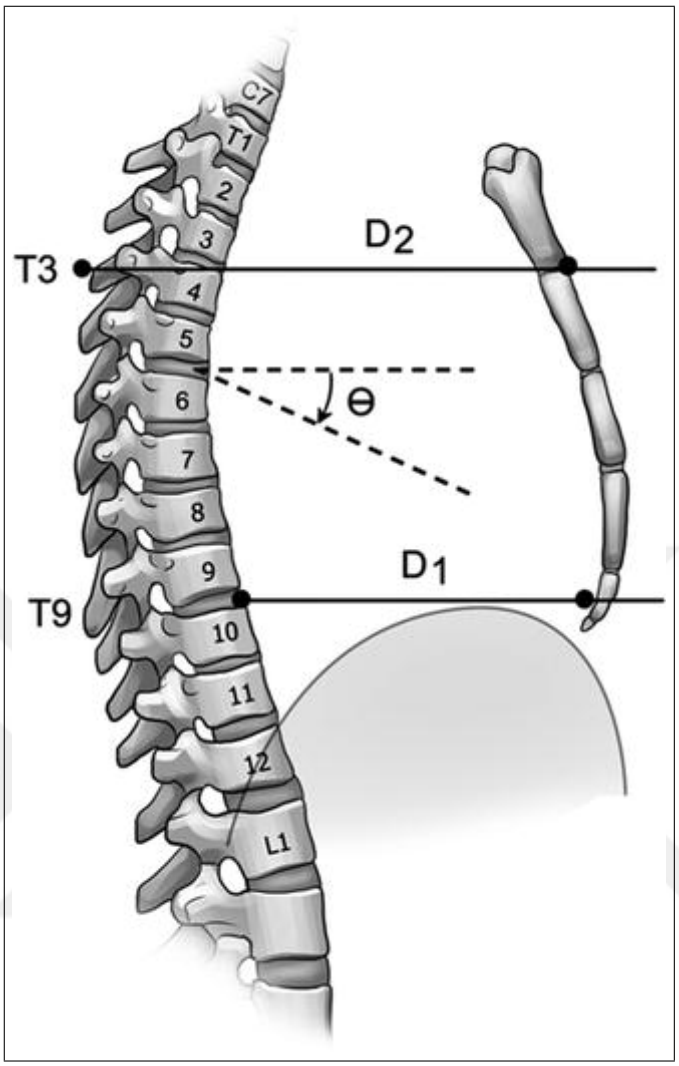

Figure 2.2 The welch index [48].

the vertebra on thorax CT; in normal humans, the value is 2.56 ± 0.35. If the value is above 3.25, there is an indication for operation [44].

In addition, the symmetric index and sternal rotation angle is measured by measuring the thorax CT sections [50],[51]. The ratio of the anterior-posterior diameter of the right inner chest and the anterior-posterior diameter of the left inner chest gives the symmetry index (in Figure 2.3). A symmetry index value of 1 indicates that the thorax is symmetrical. Symmetry index values between 1 and 0.95-1.05 except 1 deformity is slightly asymmetric; A value of 1.05 and greater than or equal to 0.95 or less indicates that the deformity is severely asymmetric.

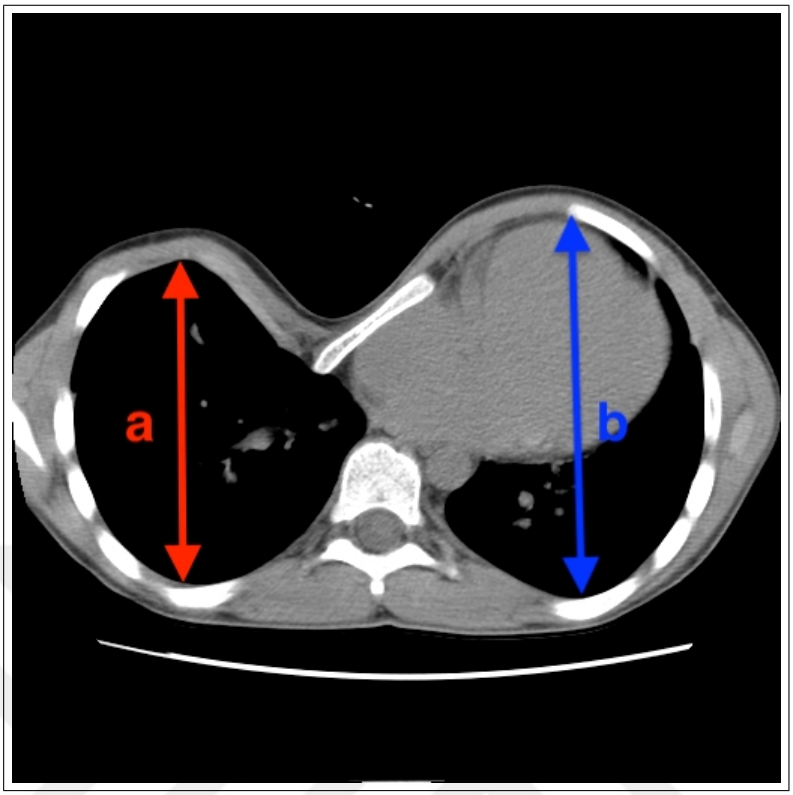

Figure 2.3 The symmetry index measurement over the thorax CT. CT image adapted from [5].

In the section where the pectus deformity is most depressed, the angle of the sternum with the horizontal plane gives the angle of sternal torsion (in Figure 2.4). If the sternum is torsion anticlockwise, this indicates that the chest wall has deformity on the right side and the angle is expressed as positive, whereas if the sternum is torsion clockwise, the chest deformity is on the left and the angle is expressed as negative. Sternal torsion angle value; It is symmetrical between 00-50, mild torsion between 50-250 and severe torsion between 250 and more. Mild and severe torsion also indicates an asymmetric case of pectus excavatum.

ECG and ECHO are important for cardiovascular evaluation. Abnormal structures such as conduction blocks, arrhythmia, right axis deviation, ST wave irregularity, and ST wave irregularity are common in patients with pectus excavatum. It may also show compression of the right ventricle and main pulmonary artery, decreased pulse volume, and decreased cardiac output. MVP (mitral valve prolapse) may be seen in 20% of the patients. Most of the findings other than MVP may be due to displacement,

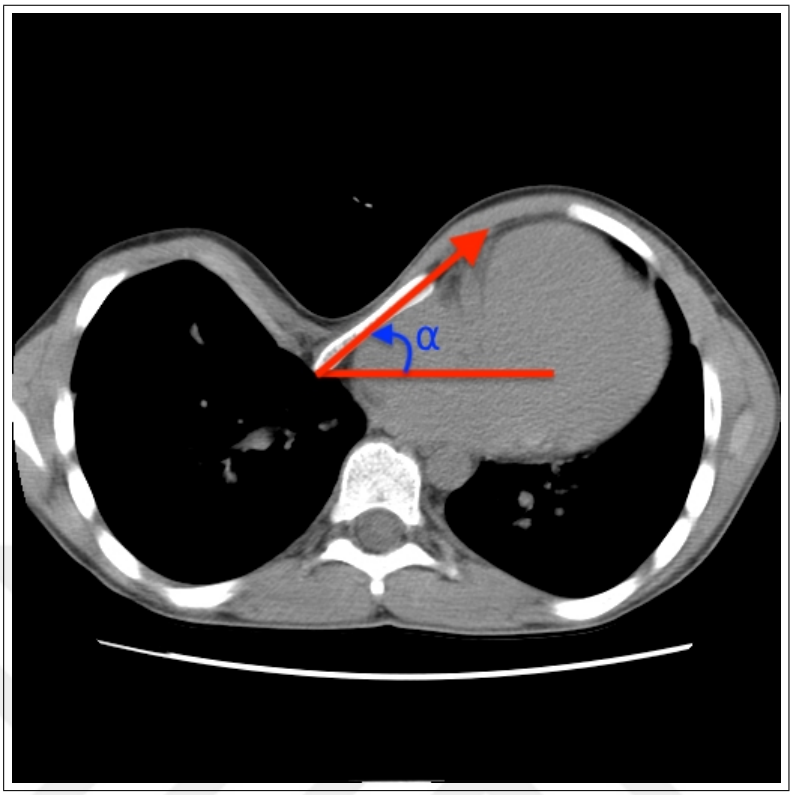

Figure 2.4 The angle of sternal torsion. CT image adapted from [5].

not as a result of actual dysfunction of the heart or large vessels. In addition, it was reported that 43% of MVP improved with correction of deformity and increased heart rate with effort [52].

In patients with pectus excavatum, the dilatation capacity of the lung causes extraparenchymal restriction by limiting the chest deformity and therefore restrictive changes in pulmonary function tests are observed. Correction operation increases the vital capacity by 10%, while improvement in maximum voluntary ventilation is more pronounced [52]. Although it is rare, allergic reactions to the components of the bar may occur in atopic individuals, so preoperative skin patch test and measurement of IgE levels may predict this complication. The presence of IgE does not indicate that an absolute allergic reaction will develop, but is only valuable in detecting sensitivity [53].

2.3 DICOM

The Digital Imaging and Communications in Medicine (DICOM) standard defines the file format designed by the National Electrical Manufacturers Association (NEMA) to help spread medical imaging systems. This format is an extension of the previous NEMA standard. This standard arises from the fact that hospitals and doctors in different locations and with different functions need a structure in which they can share in a common language. It is also a particularly recommended standard for the creation of a common platform where the manufacturers of devices for which medical images are obtained will have a competitive chance. Considering that this standard does not exist, the software used by the device is compelled to process the medical image produced by the device. In addition, the formation of a common structure, information can be obtained and processed quickly and easily by those in need. It is the standard file format developed for medical images. However, it does not have similarity with known file formats. For example, Joint Photographic Experts Group (JPEG) file contains only a single image information and Exchangeable Image File Format (EXIF) information where DICOM files contains large set of metadata along with multiple raw images. This information is the basic format descriptor, such as the application, related versions, and character set that make up the file. In addition, DICOM files, if desired, can contain patient information and detailed information (in text) related to the relevant image. It can also be stored in Multi-Frame (3D) images within the DICOM format. The main purpose of this standard is to store all the required data such as hospital information, medical device information and patient information [54].

3. METHOD

3.1 Requirements and Specifications

This thesis aims to design software and hardware tools for shaping pectus bars in order to assist surgeon in pectus excavatum operations. To fulfill the quest we followed Biodesign process. Biodesign innovation process was the outcome of the eight years of experience of biodesign innovation and fellowship programs at Stanford University [55]. We followed the plan of three main parts (identify, invent, implement) which is shown in Figure 3.1.

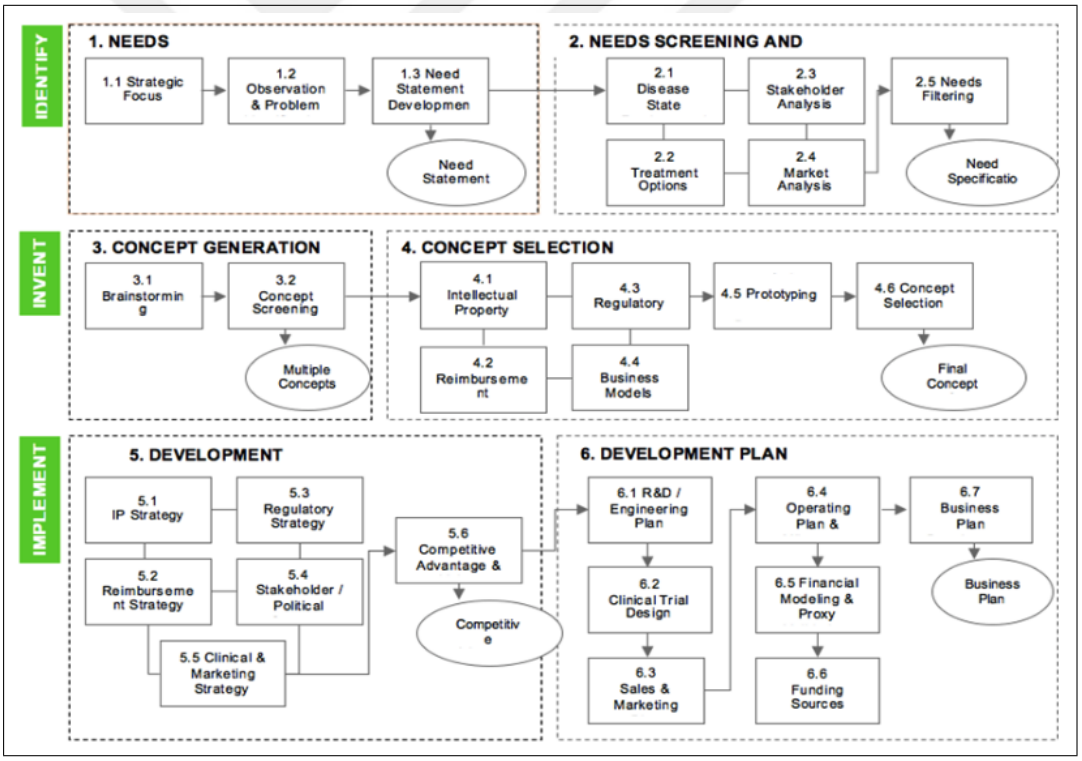

Figure 3.1 Biodesign innovation process, adapted from [55].

First step was to identify the needs; in which exists 3 subsections of effort to find a need statement. Below is the summary of what we did in the first stage:

1. Strategic Focus

   Within the scope of the project strategic focus, were determined with the support of academic advisor, medical doctor and the literature review [46],[47].

2. Observation, Problem Identification and Need Statement Development

   Observation and problem Identification was defined by the surgeon who routinely performs the Nuss operations. The problem defined by the surgeon also constitutes the objective sentence of the thesis.

3. Disease State Fundamentals and Treatment Options

   These are explained in detail at the chapter 2.

4. Stakeholder Analysis

   Stakeholder is defined as the group that actively participates in the production of the product and is directly affected by the results of the product [56]. Stakeholders identified for this project are medical doctors, thesis advisor, student and patients. Each of these stakeholders is directly affected by the new product design.

5. Market Analysis

   Market analysis was obtained by multiplying the frequency of the disease and the prices of the products used during surgery. It has been reported in the literature that this disease occurs between 0.1% and 0.4% of the population [47]. Advisor medical doctor stated that the price of the products used is 2000 USD, since the market is 7.53 billion people, the market analysis results are obtained by the help of Eq. 3.1 and Eq. 3.2.

$$Market\ Volume_{Start\ of\ interval} = 7.53 * 0.1\% * 2000 \tag{3.1}$$

$$Market\ Volume_{End\ of\ interval} = 7.53 * 0.4\% * 2000 \tag{3.2}$$

The market volume was calculated as between $15.06 billion to $60.24 billion.

6. Needs Filtering, Ideation and Brainstorming, Concept Screening, Intellectual Property Basics

   The definition of the needs was made by the medical doctor, the ideation and brainstorming was made by the thesis advisor, the student and the medical doctor, the concept screening was made by the thesis student, and the intellectual property basics was done by the thesis supervisor.

7. Regulatory Basics

   For the regulation part Medical Devices Agency of Turkey (TTCK) records are examined for the similar manual devices that does the same operation. As a result similar devices are used in Turkey with United Nations Standard Products and Services Code (UNSPSC) 4229000.

8. Reimbursement Basics

   Since the mode of operation has not changed, the consultant surgeon has indicated that existing payment systems can be used as payment methods. These methods of payment are in the form of pay by cash in private hospitals and the payment of a certain percentage by the state in public hospitals.

9. Business Models

   After clinical testing of the product, the business model will be decided. However, pre-production is considered as the main business model.

10. Prototyping

    Details on prototyping are described in chapter 3.

3.2 Mechanical Design

3.2.1 Automated Bar Bender Design

The chassis design is one of the most important parts of the entire system. For this type of design to be portable, easily developed and robust, materials that are as durable and suitable for modular construction should be selected. Considering these criteria, 4-channel aluminum sigma profile stands out. This profile is preferred in many environments with its mounting advantage, light weight and robustness. If required, it can be used before surgery and if necessary, during the operation to meet urgent needs. Figures 3.2, 3.3 and 3.4 provide information about the outline of the chassis.

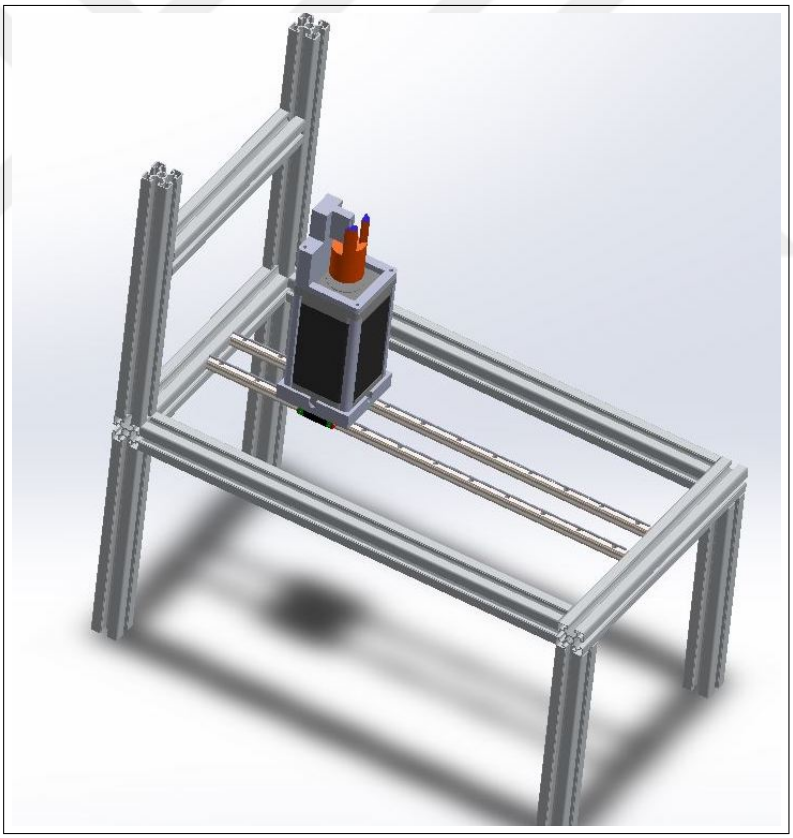

Figure 3.2 The outline view of the chassis.

The frame is basically mounted on 2 horizontal sigma profiles to reduce vibration and shaking. It is aimed to allocate the necessary space for the motor and drivers by

Figure 3.3 The side view of the chassis.

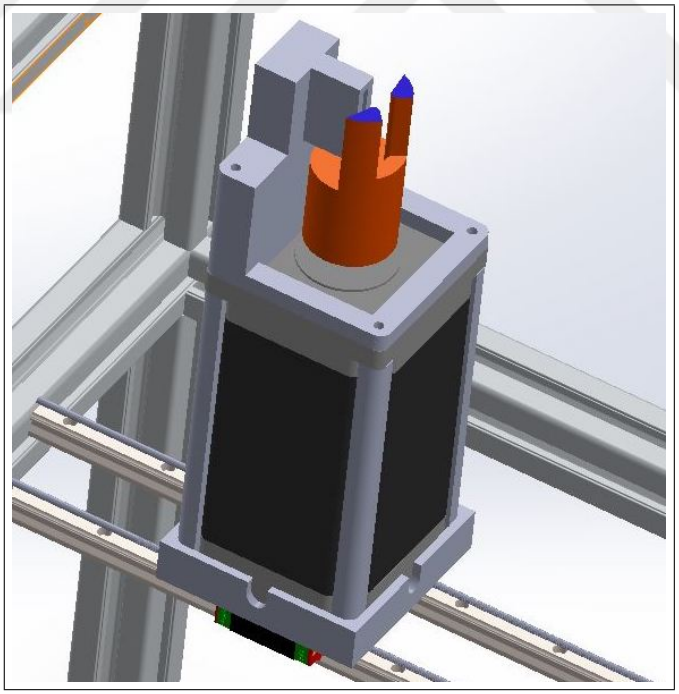

Figure 3.4 The zoomed view of the chassis.

placing a certain height on these legs. On the upper side, there is an adjustable height where the bar is to be fixed and the area where the linear belt system will be placed.

3.2.2 Bender Head Design

Several concepts have been tried to design the bending head. However, most of them suffered from low strength and short turning angles. In the first stage, a design was made of 6 holes which can be fitted with 2 pins as shown in Figure 3.5. However, the variation offering the highest angle of rotation was chosen due to insufficient strength. This angle is calculated from the bending point, the applied force point and the torque gained. The technical drawing of final design of the bender head is shown in Figure 3.6.

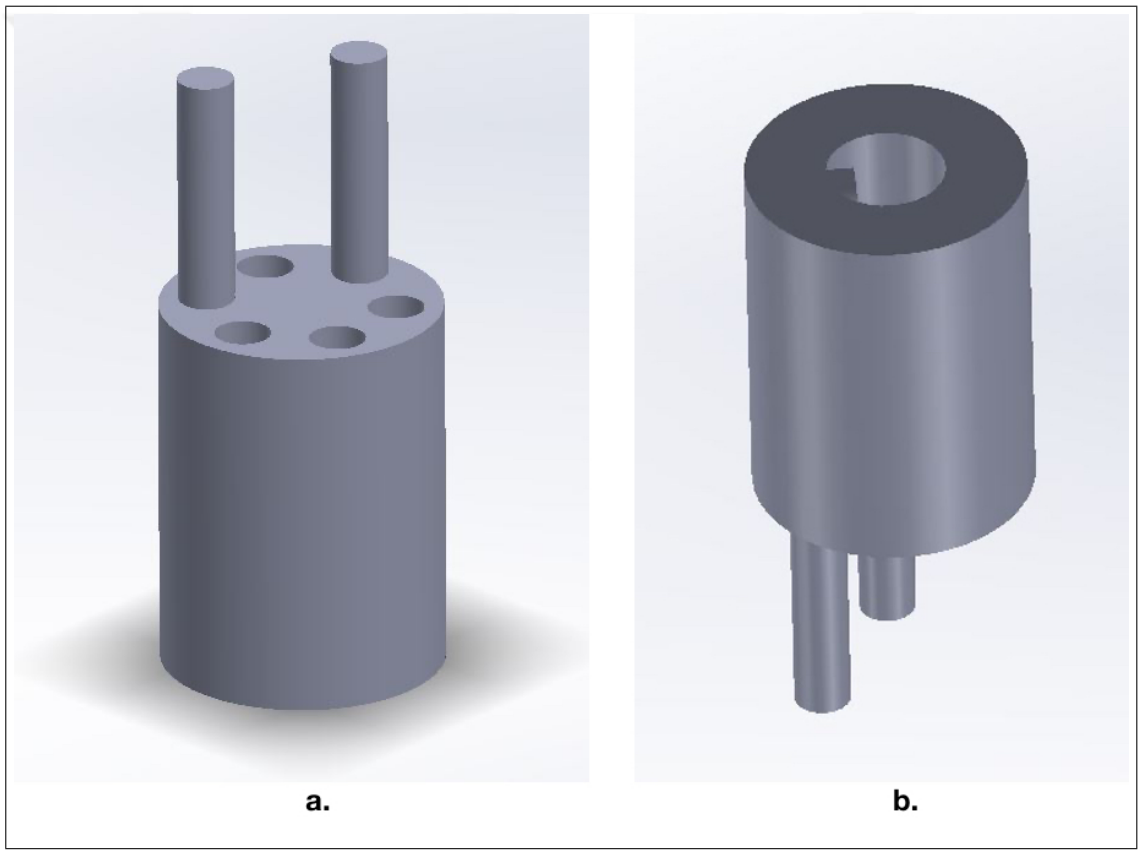

Figure 3.5 The first design of 6 holes bender head (a.Top view b.Bottom view).

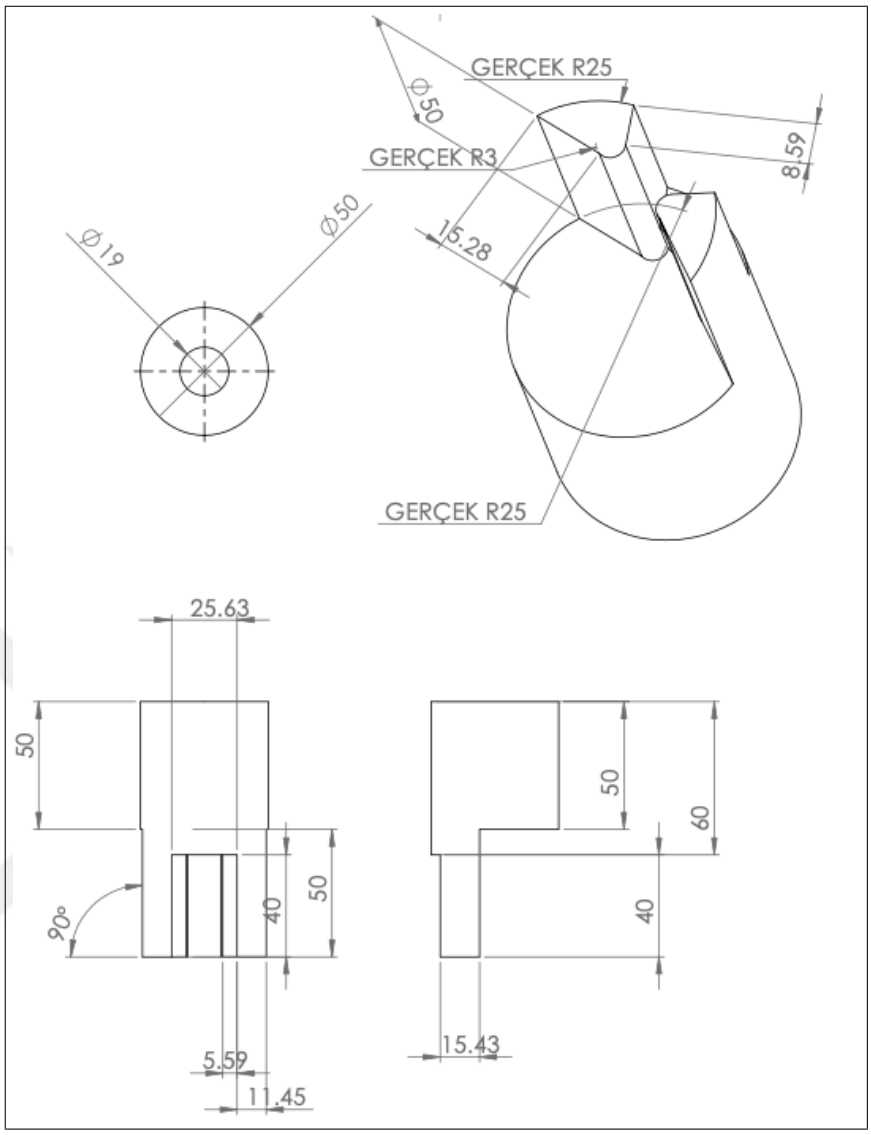

Figure 3.6 The technical drawing of the bender head.

3.2.3 Motor Holder Design

The system is designed to absorb most of the load caused by rotation on itself. Therefore, the skid structure connecting the motor to the linear belt and the motor holder connecting the motor to the skid must be of strength. Custom teflon polytetrafluoroethylene (PTFE) part was manufactured by means of a CNC used in wood processing to keep the engine fixed on the slide. The motor holder is fixed on the cradle with 4 screws. The drawings of the motor holder are given in Figure 3.7.

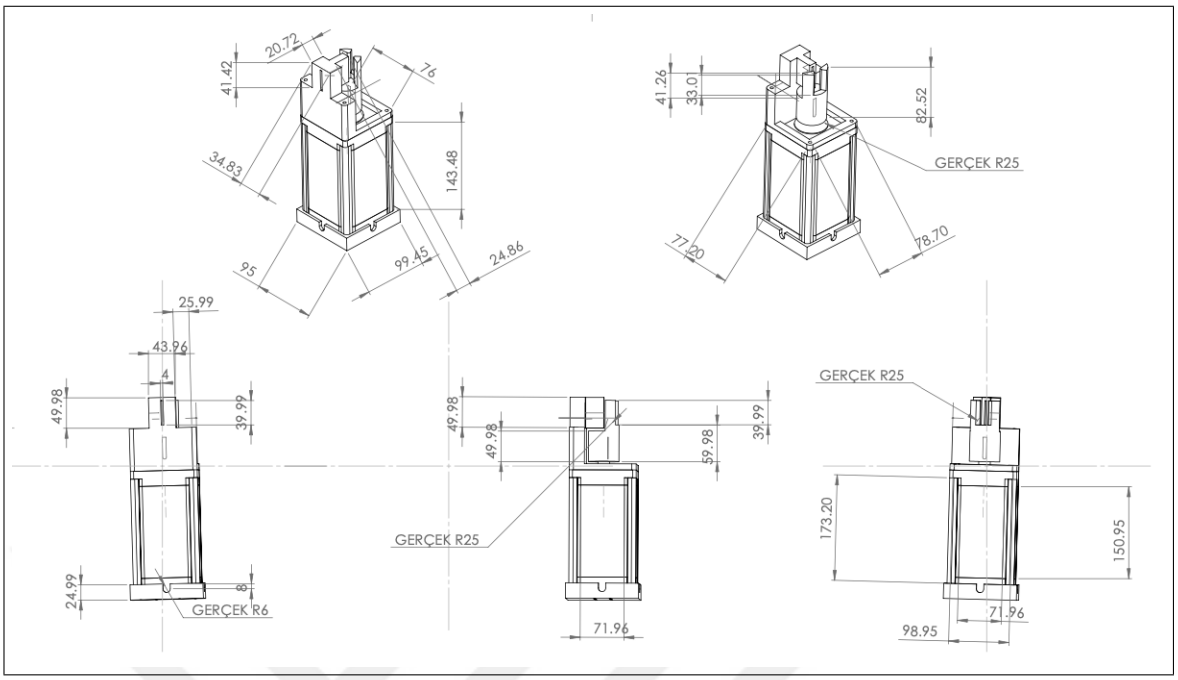

Figure 3.7 Technical drawings of the motor holder.

3.2.4 Linear Timing Belt Module

A module was needed to provide linear movement of the main motor in the designed system. In order to meet this need, linear timing belt has been chosen as the most appropriate option. Detailed information about this module is given in the following sections.

3.2.4.1 General Specifications. In required applications, high speed and precision, the series of timing compact modules are preferred. Thanks to their closed designs, these series are suitable for working in dust and particulate environments. In our application, it will be used to carry the main motor that will perform the bending action and to provide twisting from different points by moving this motor linearly. The view of this module is shown in Figure 3.8

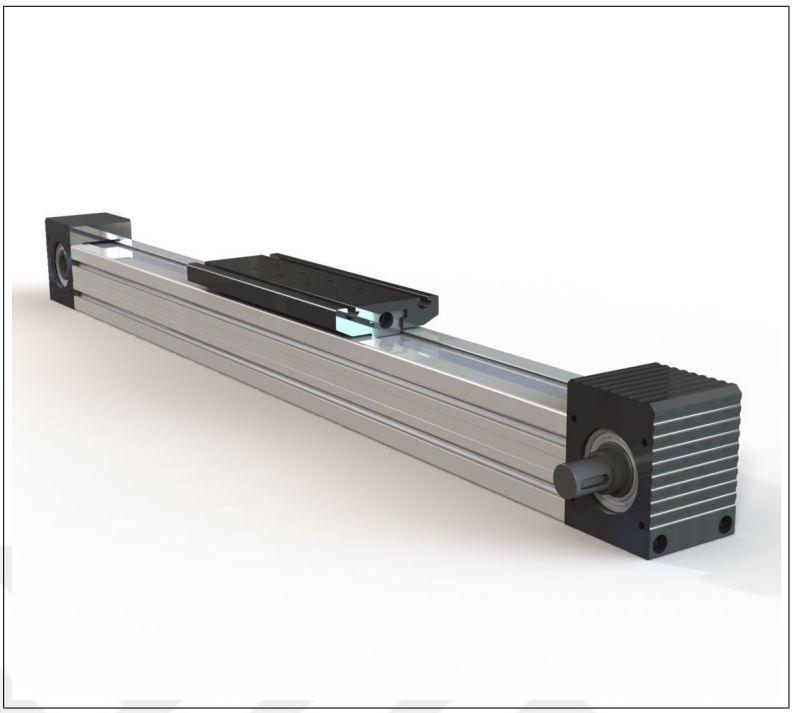

Figure 3.8 The view of linear timing belt module [57].

3.2.4.2 Technical Specifications. This series, which is small in size, can be preferred for designs with space problems. With this system, high speed can be achieved in the applications with low load capacity, thanks to the design of the trigonomous drive system. Technical specifications of this module are given in Table 3.1.

Table 3.1
Technical specifications of the linear timing belt module [57].

Specification	Value
Body	64x64 Section (Aluminum 6063) T5
Displacement per revolution	130mm
Timing Belt	5M-F30 Z=26
Pulley Tensile Force	2000N
Belt Pitch	5mm
Positioning Accuracy	0.1mm

The technical drawing of the linear timing belt is given in the Figure 3.9.

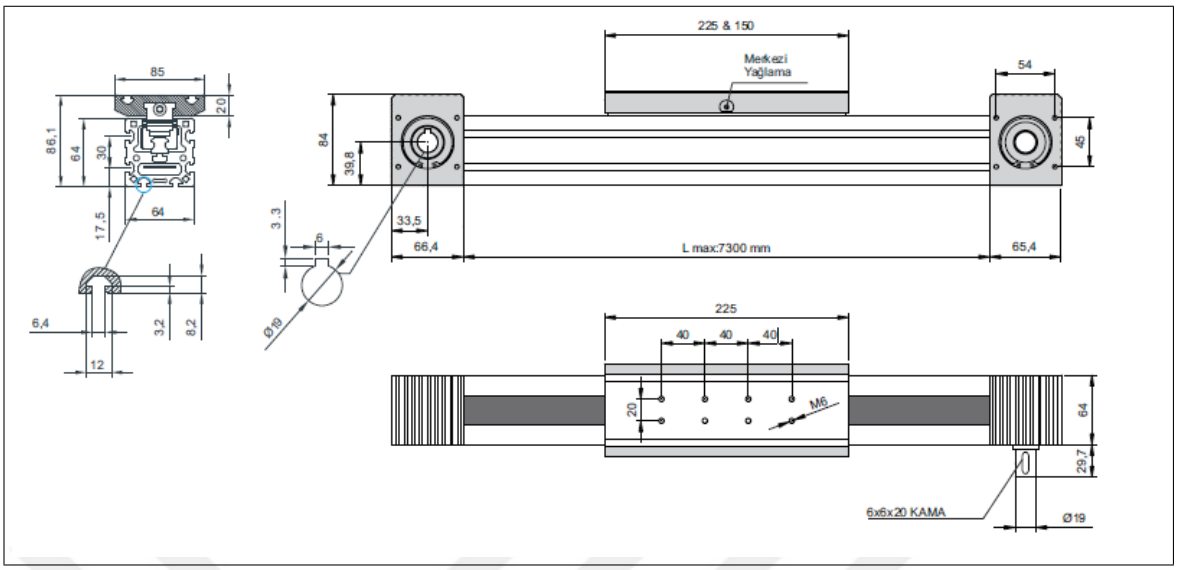

Figure 3.9 The technical drawing of linear timing belt module [57].

3.2.4.3 Loading Capacity. Load capacity values for linear timing belt and the axes to which they belong are shown in Figure 3.10.

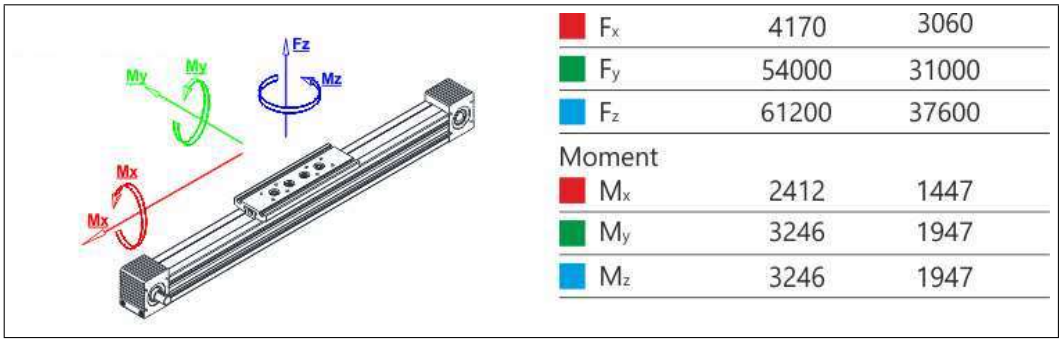

Figure 3.10 The load capacity values of linear timing belt module [57].

3.3 Electrical Design

3.3.1 Microprocessor

As microprocessor ESP8266 was chosen to have a compact design and WiFi connectivity. ESP8266 offers efficient power usage and minimalist design to users especially in Internet of Things (IOT) applications. Moreover, the microprocessor has integrated WiFi and ability to work master or slave device depend on the application. Although ESP8266 is a low-cost device, it has better specifications among its competitors. It contains a 32-bit processor and on-chip SRAM. The SDK provides example codes and built-in functions to enhance development process [58]. The PCB layout of the module is shown in Figure 3.11. The microprocessor controls the motor drive unit by sending PWM signals to the unit. At the beginning ESP8266 receives the point list to be bent. After the arrival of the point data microprocessor determines the required angle for next bending point and converts that angle data to PWM signals. The module schematics of ESP8266 is shown in Figure 3.12.

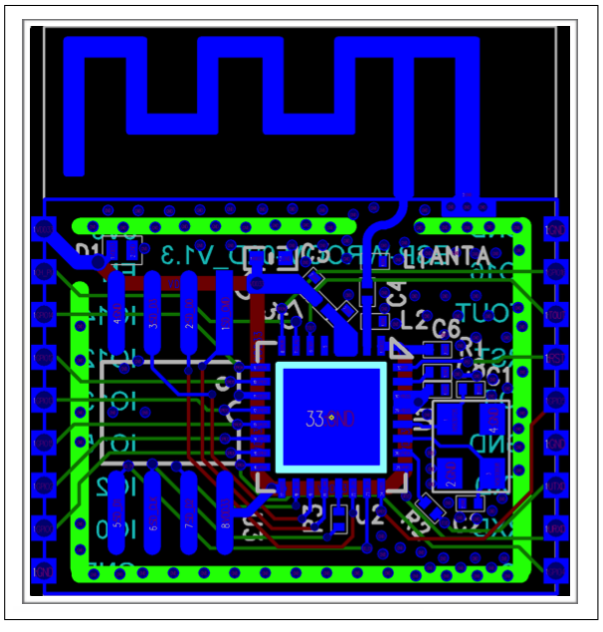

Figure 3.11 ESP8266 PCB layout [59].

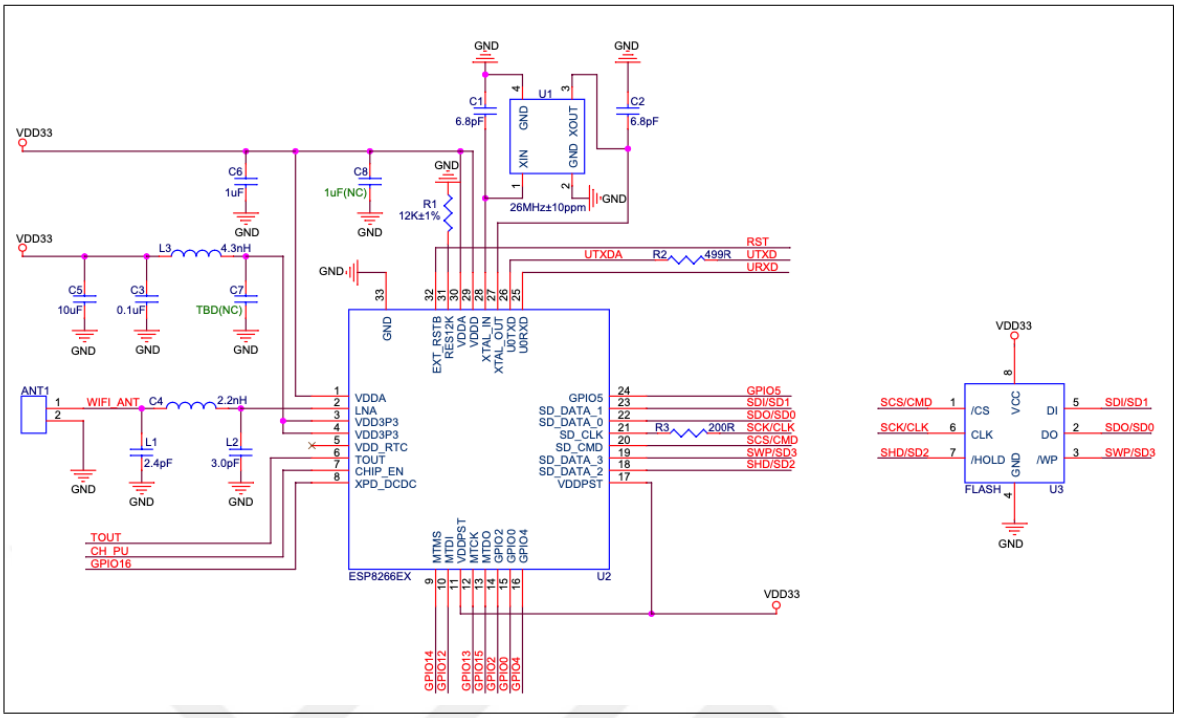

Figure 3.12 The module schematics of ESP8266 [59].

3.3.2 Motor Specifications

As torsion motor 110HS28 model generic motor with 28 Nm torque, which are built based on NEMA-42 motor dimension standard, was selected. The motor is a stepper type motor which has 200 stator poles for every 1.8 degrees of angle. Selecting this kind of motor is both advantageous and disadvantageous. Stepper motor is easy to control due to high sensitivity. However, these motors does not offer as much power as equivalent DC motors. This motor is chosen due to lower cost in comparison to its competitors. Motor specifications are given in Table 3.2.

The wiring connections diagram of the motor is shown in Figure 3.13 and dimensions of the motor are given in Figure 3.14.

Table 3.2
The specifications of 110HS28 [60].

	Holding Torque (2 phases on) N.m(min)	Rated Current/Phase (Amps DC)	Resistance /Phase (ohms) ±10%	Voltage /Phase (V DC)	Inductance /Phase (mH)±20%
Unipolar	20	5.6	1.3	7.28	12.7
Bipolar(Series)	28	4.0	2.7	10.8	50
Bipolar(Parallel)	28	7.8	0.65	5.07	12.7

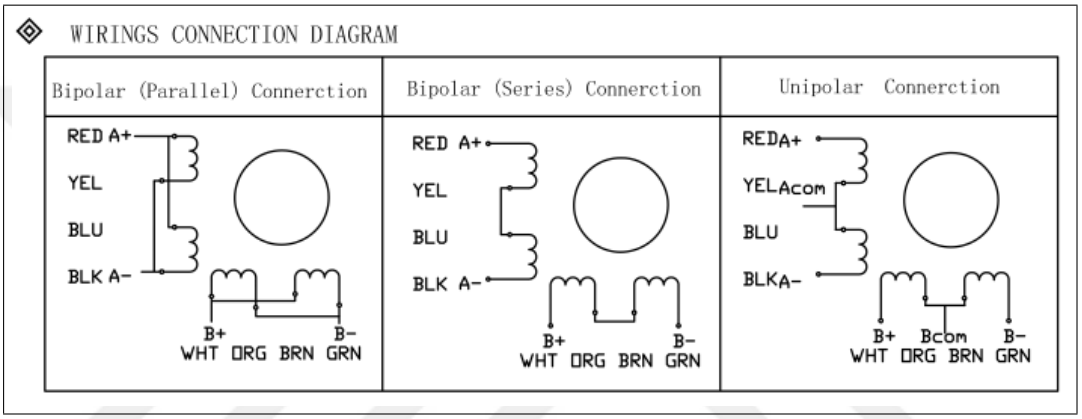

Figure 3.13 The wiring connection diagram of the motor [60].

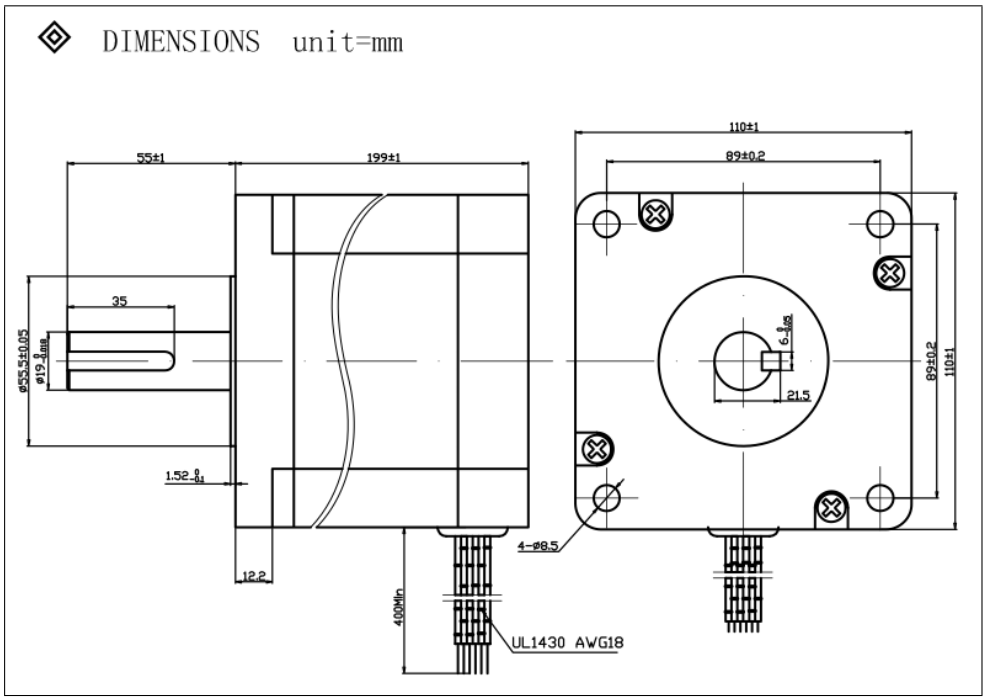

Figure 3.14 The motor dimensions [60].

3.3.3 Motor Drivers

In this project, since two stepper motors with different power ratings were used, two separate motor drivers were needed to drive these motors. These are CW2283 Stepper Motor Driver and CWD556-A Digital Stepper Driver.

3.3.3.1 CW2283 Motor Driver. CW2283 (in Figure 3.15) is high performance stepper motor driver for two-phase and four-phase stepper motors. The driver has also micro-stepping capability. This allows us to use motor full step to 51200 steps/rev. The working current interval of the motor driver is between 2.0A and 8.3A [61]. The electrical specifications of the stepper motor driver is given in Table 3.3

Table 3.3
The electrical specifications of the CW2283 [61].

Parameter	Min	Typical	Max	Unit
Input Voltage(AC)	150	-	220	V
Output Current	0	-	8.3	A
Pulse Signal Frequency	0	-	200	kHz
Logic Signal Current	7	10	16	mA

Figure 3.15 The CW2283 motor driver [61].

The typical connection diagram of the stepper motor driver is given in Figure 3.16.

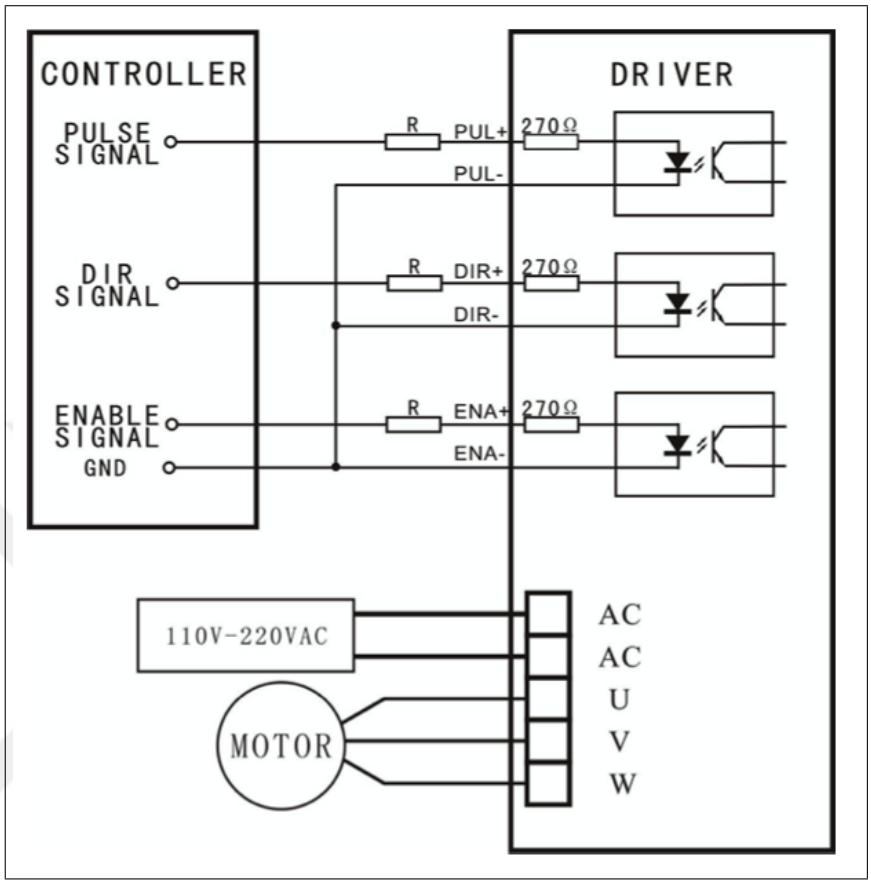

Figure 3.16 The connection diagram of CW2283 motor driver [61].

3.3.3.2 CWD556-A Motor Driver. The CWD556-A is a digital 2-phase new generation stepper motor driver. Some of the features of this driver can be listed as follows:

- low-noise
- high precision
- anti-resonance
- DSP(Digital signal processor)
- micro-stepping

The electrical specifications of the driver are given in Table 3.4

Table 3.4
The electrical specifications of the CWD556-A [62].

Parameter	Min	Typical	Max	Unit
Input Voltage(DC)	20	-	50	V
Output Current	0	-	5.6	A
Pulse Signal Frequency	0	-	200	kHz
Logic Signal Current	7	10	16	mA

The typical connection diagram of the digital stepper motor driver is given in Figure 3.17.

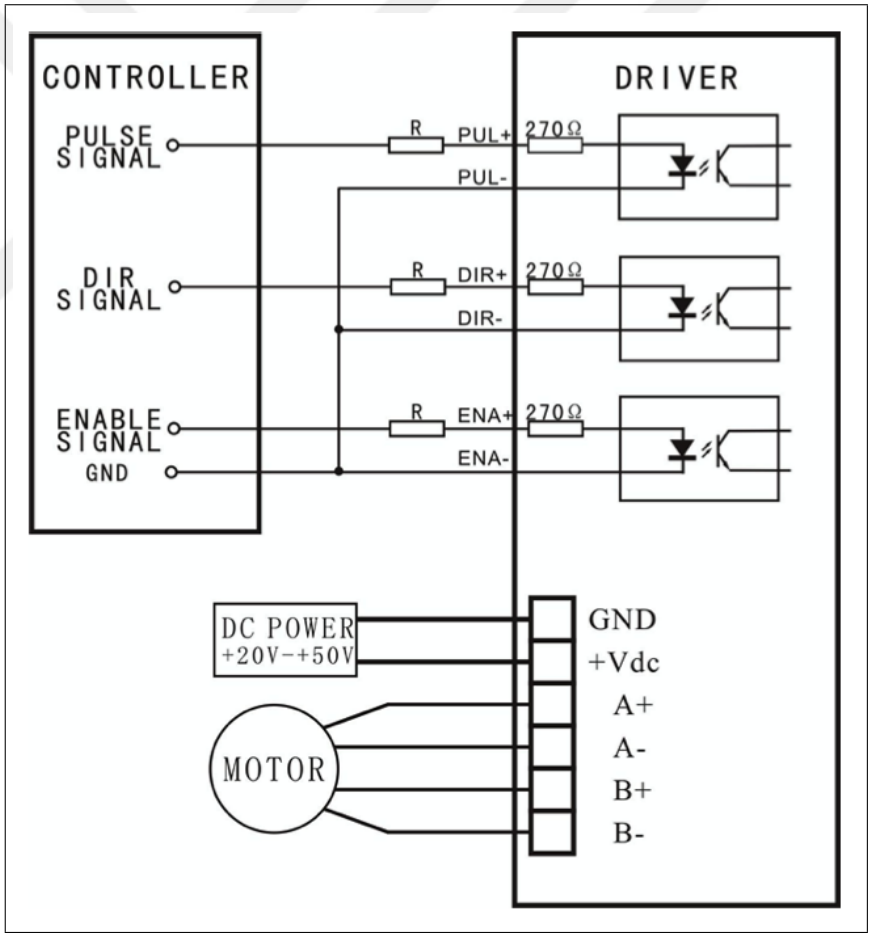

Figure 3.17 The connection diagram of CW556-A motor driver [62].

3.4 Software Design

3.4.1 Back-end

3.4.1.1 Programming Language Selection. Javascript is a programming language to manipulate websites on the browser. It was created by company called Netscape to use in their browser Netscape Navigator. Although there was an attempt to make javascript a back-end language in the past, the attempt was not successful due to technological infrastructure at that time. With the rise of modern Web 2.0 applications like Gmail javascript gained more popularity and the technological improvements in the server-side hardware result with the creation of NodeJs. NodeJs is a powerful back-end language based on javascript. It brings the server side rendering and operations based on javascript that formerly a front-end language [63].

Although, Python was used as back-end language at the beginning of the project, we had to convert our code to NodeJs for better compatibility and performance.

3.4.1.2 Integration DICOM with NodeJs. We used Thorax-CT data of the patient to provide an overview of the patient condition to doctors. Moreover, the desired final geometry shaped of the bar is drawn on the CT data which selected by the doctor. CT and similar medical imaging platforms are using DICOM standard.

The standard specifies the unified way of collecting and storing required patient data. The data is written on specific bytes on the DICOM file and the byte reference is also stated in the standard. Since, the DICOM files are stored in the binary format and it is not common like the other image types like JPEG and PNG there is no standard library for it. Since the DICOM files contains high density of data, their file sizes are considerably larger than other imaging formats. For example one of the sample dataset that we used contains 180 mb of raw data. For that reason, the challenging part is the parsing and displaying data with efficient resource usage. To achieve that goal asynchronous programming techniques are used to parse data.

First, the DICOM files loaded via browser. After the files are loaded into browser cache, files are scanned, processed one by one and added to file buffer. In the next process, the pixel array is splitted from the data which is located at the byte at x7FE00010 [64].

In pixel array, the pixels are encoded from left to right, top to bottom which means each row given in order. Considering the pixel array is an flat type array, the image data has to be converted to a matrix as the next procedure. On the other hand, pixel array itself does not contain enough information for that conversion. To form the matrix, image width and height properties are extracted from the DICOM metadata. After that part, other required metadata is extracted and sent to front-end for further conversion.

3.4.2 Front-end

3.4.2.1 Framework Selection. Vue.Js javascript framework was preferred as the front-end interpreter. VueJs is a reactive framework which handles component updates based on the variables states and properties. The features of the framework decreases the production time of the front-end application while increasing application performance and reliability.

3.4.2.2 Components. The front-end module has three main components called Table, Designer and Main. The Table component handles the patient metadata, parses it and keeps itself updated on metadata change events. The change events are fired externally outside of the component then it fires the update life-cycle of itself. At the Designer part there are several elements and various functionalities are encapsulated. First at the design container, which is built on HTML canvas and shown with the higher z-index than CT image container, handles the drawing process. The next one is the image display layer located under the design canvas, is responsible for containing the current CT image. Since design canvas has a transparent background, the CT

image can be seen easily. The last component is Main which manipulates the data flow between its child components.

3.4.2.3 Forming Transverse and Sagittal Images. For the forming stage sagittal and transverse images from pixel array that we have created earlier, it is needed to loop 3 dimensional pixel array. For the reason of having multiple images at the same time, each image has to be processed individually. In that processing part the median vector from the transverse image (Figure 3.19) is taken and written to the sagittal (Figure 3.18) image canvas.

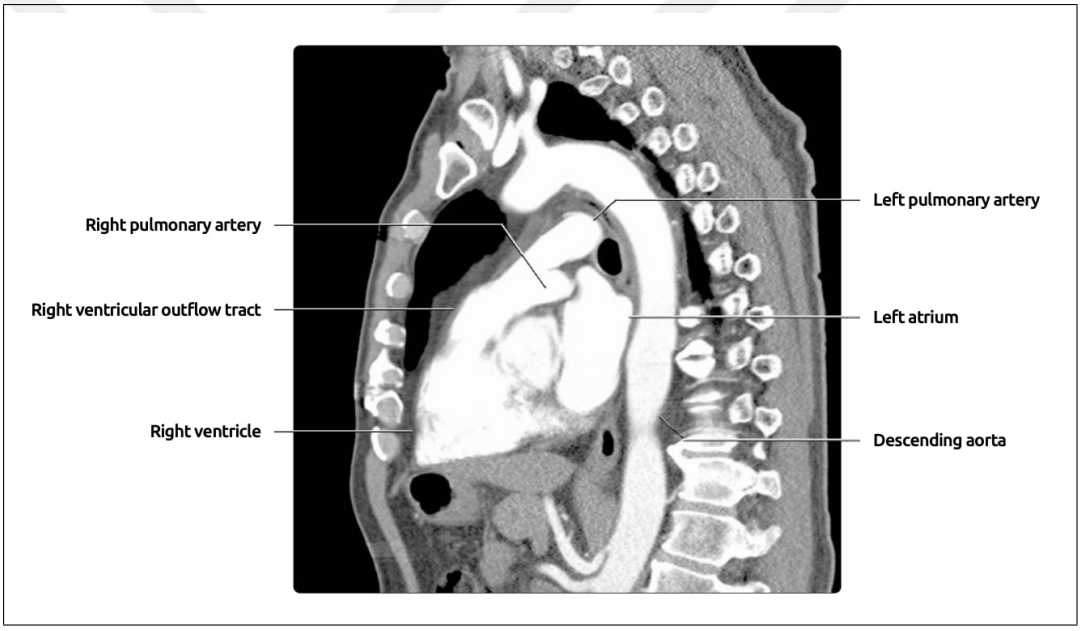

Figure 3.18 The example sagittal view of a CT image [65].

3.4.2.4 Drawing Bèzier Curves. The method used to draw the bar shape of the users is the Bezier curve equations. Unlike most other curve fitting methods, when the control points are determined, the equation of the bezier curve is constant and the calculation method does not change. It is widely used in graphical computational programming languages with small number of points that can be easily manipulated by the user in computer graphics.

A Bèzier curve (also known as B-B curve) is a polygon defined by Bèzier-

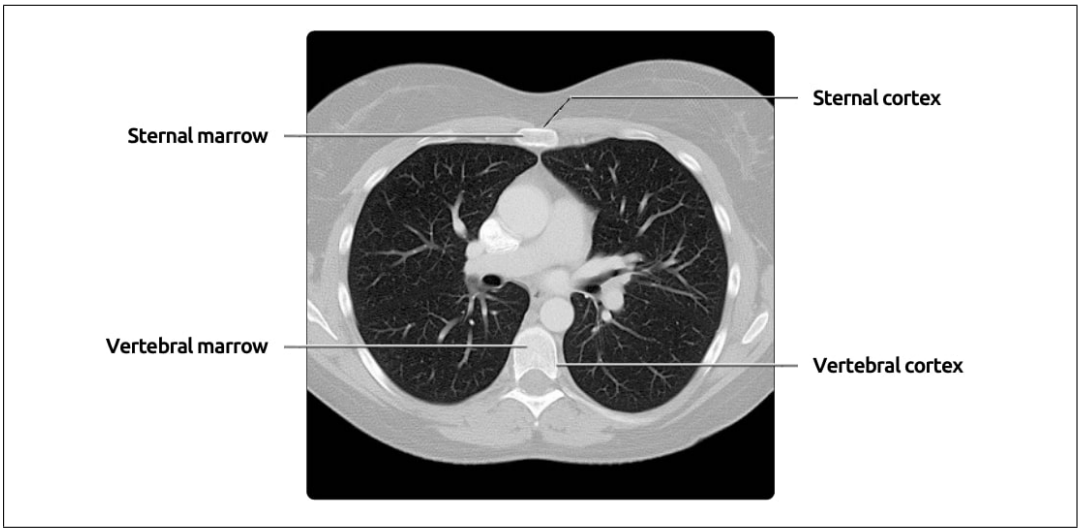

Figure 3.19 The example transverse view of a CT image [65].

Bernstein polynomial. This polynomial describes cubic and quadratic splines which consist of 3 control points in quadratic 4 control points in cubic Bèzier curves. Each polynomial is evaluated for the values between t = [0,1] in which are given in Eq.3.3 and Eq.3.4 [66].

$$P(t) = (1-t)^3 V_0 + 3t(1-t)^2 V_1 + 3t^2(1-t)V_2 + t^3 V_3 \tag{3.3}$$

$$P(t) = t_2(V_0 + V_1 - 2V_2) + t(2V_1 - 2V_0) + V_0 \tag{3.4}$$

where V_n is control points which implies (V_{x_n}, V_{y_n}).

We chose quadratic Bèzier curve for being easy to implement and user-friendly. For the displaying part, user should point the control point on the canvas. After the first selection, a pointer device event is triggered to watch the user's mouse coordinates. On every mouse move on the design canvas, the assigned event triggered and whole canvas is redrawn with the updated points. At that while, a set of events are also set for watching the browser named "mousedown", "drag" and "keypress" to understand the

next occurrence of user input. On mousedown event user sets a permanent control point and events are set to watch the next action. On keypress event only the ESC button on the keyboard is being watched to remove last control point. After the drawing process is completed or if there is an error in curvature or the location in the curves, user can drag any control points to form final bar geometry. Various Bèzier curves with different control points are shown in Figure 3.20.

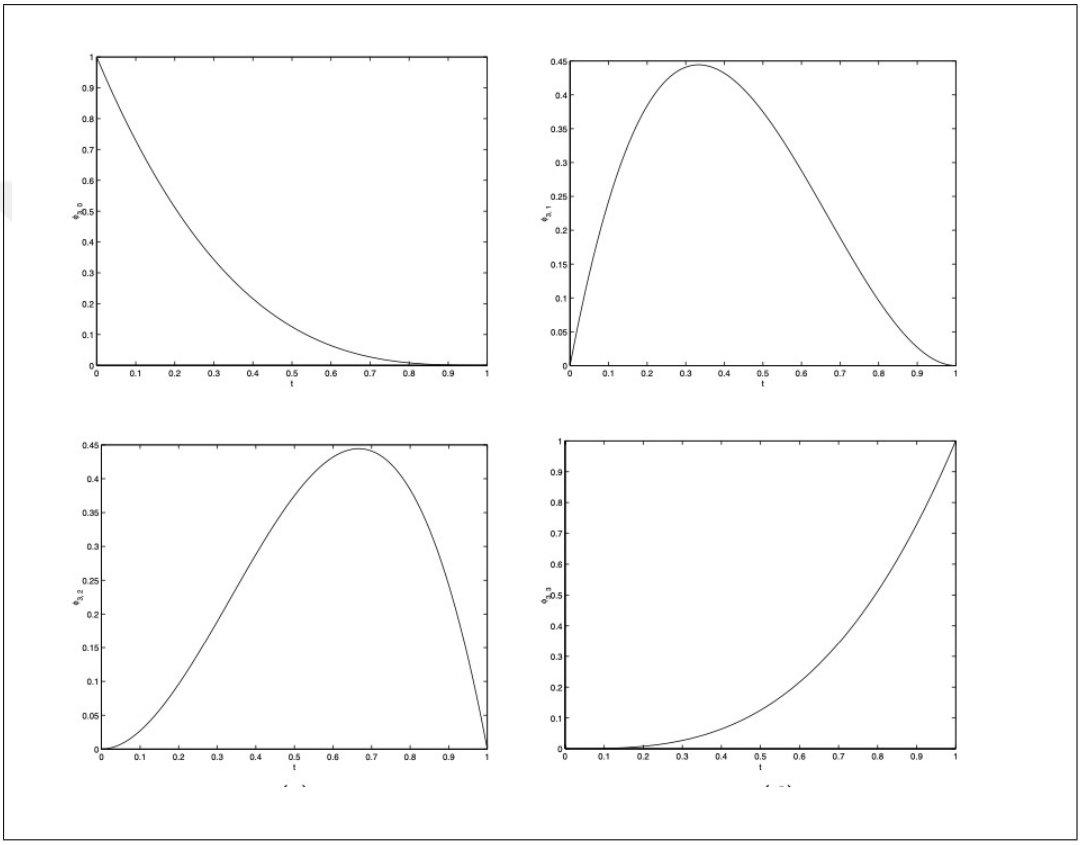

Figure 3.20 Various Bèzier curves with different control points. Adapted from [66].

3.4.2.5 Sampling Data Points. The formula of the cubic Bèzier curve in Eq. 3.5 was used to extract the sample of the data points.

$$\begin{aligned} P_x(t) &= (1-t)^2 * P_{1_x} + 2 * (1-t)t * P_{2_x} + t^2 * P_{3_x} \\ P_y(t) &= (1-t)^2 * P_{1_y} + 2(1-t)t * P_{2_y} + t^2 * P_{3_y} \end{aligned} \tag{3.5}$$

Since the sensitivity to required depends on the clinical condition of the patient,

the sampling rate of the bar was initially left undetermined. However, in view of the physical limitations and in order not to create an extra layer of twist accuracy, it would be appropriate to have a sample size of no more than 140 for a 70cm bar. This implies a resolution of approximately half a centimeter, which is not available to handpieces and bending tools currently used. For other bar lengths, the required number of samples can be found by making a proportional calculation. However, only as a suggestion, the system assigns the default value which can be changed later according to the entered bar length.

3.4.2.6 Pixel to Actual Length Calculation. Mathematical approaches could be used to calculate the actual length between 2 points (in Figure 3.21), but since any point of the curve can be calculated, after sampling over the number of curves allowed by the system resources, a very narrow distance between 2 points in each delta(x), delta(y) interval is calculated and the total distance between points is calculated.

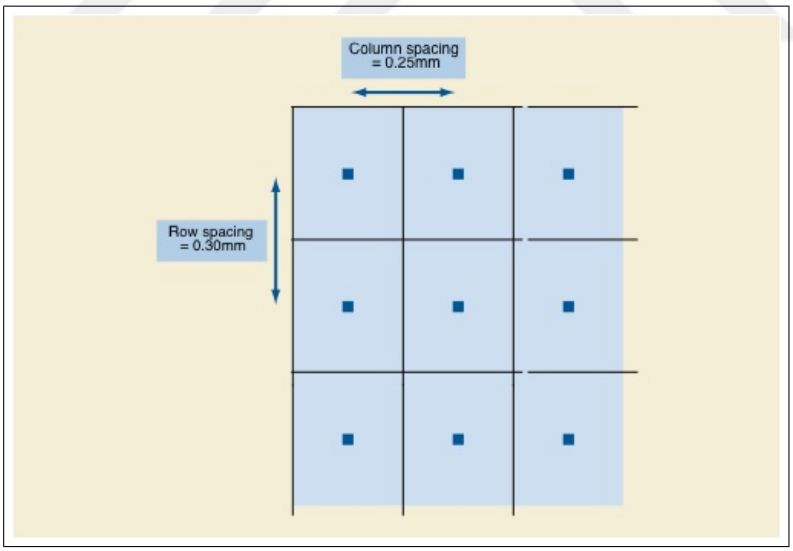

Figure 3.21 The example of pixel spacing value [67].

3.4.2.7 Graphical User Interface Design. The graphical interface is simple and easy to use for surgeons. It is aimed to increase the efficiency of the doctor or health care worker with these screens which do not contain many buttons. The con-

cept generally consists of 2 pages. The first page is also the home page for uploading DICOM images.

Figure 3.22 shows this home page. Figure 3.22 in the area marked with the letter "a" is the file upload area. This field allows DICOM files to be selected from the computer or dragged and dropped so that files can be uploaded to the system. In the section marked with the letter "b" in Figure 3.22, there is a small information area to inform the user about the process.

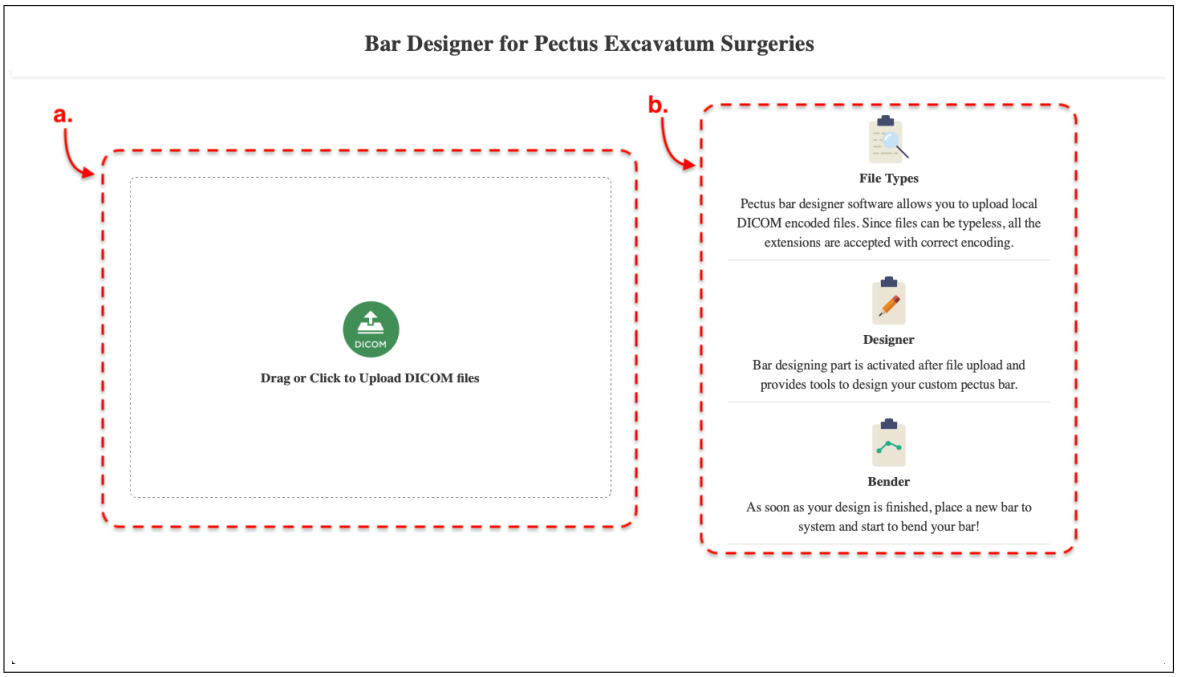

Figure 3.22 The homepage view of the GUI.

Once the files are selected, the system automatically processes the files with client-side processing methods. This means that the patient's personal data is never sent to the server for fulfilling two important criteria. The first one is to use the user's computer for transactions to reduce server costs. The second is to protect confidentiality by not sending the patient's confidential information to the server. A semi-transparent loading screen appears while processing is in progress.

The screenshot after loading is given in Figure 3.23. In this figure, the image in

the sagittal plane was obtained from this CT data which normally contains transversal images. With this sagittal observation section, the doctor can see in which plane the patient sees in two planes. In addition, mouse cursor movements in the sagittal compartment are monitored to give the transverse image at the mouse cursor position. This screen can be seen in the part of Figure 3.23 marked with a. In the same way, the field marked with b gives information about the functions. Section d is the navigation section.

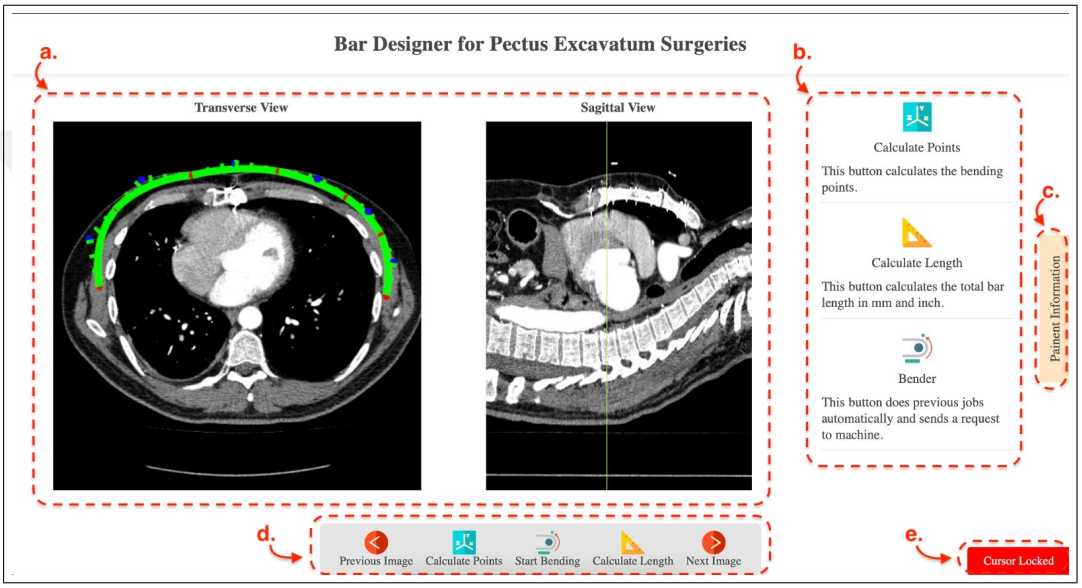

Figure 3.23 The designer view of the GUI.

In the Figure 3.23 field marked with the letter c, displays patient information on click action, related screen is given in Figure 3.24.

The detailed figure for navigation is given in Figure 3.25. The parts marked with a, e opens the previous / next picture go function, the parts marked with b and d opens the drawing points and the length calculation function, and the part marked with c opens the setup part to start the bend operation.

Figure 3.26 shows the detail of the bar design screen. In this screen, the parts marked a, b show a unit bar which exceeds the control points of cage. Also, d shows the position of the transverse image in the sagittal plane.

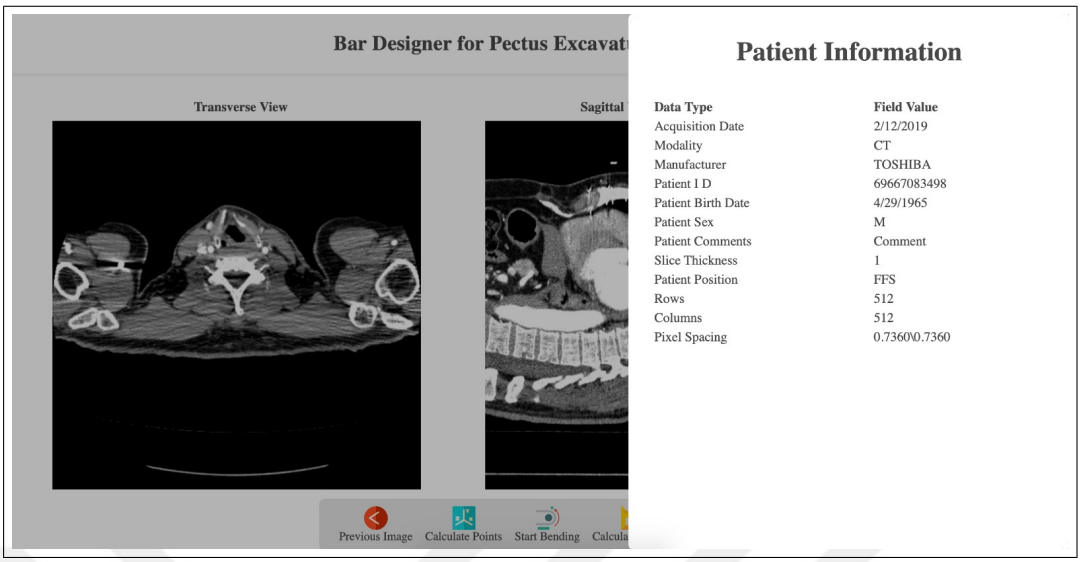

Figure 3.24 The patient information screen.

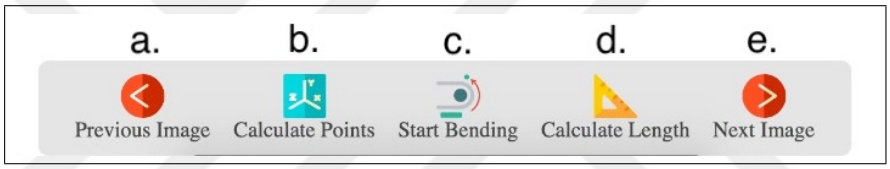

Figure 3.25 The toolbox of the GUI.

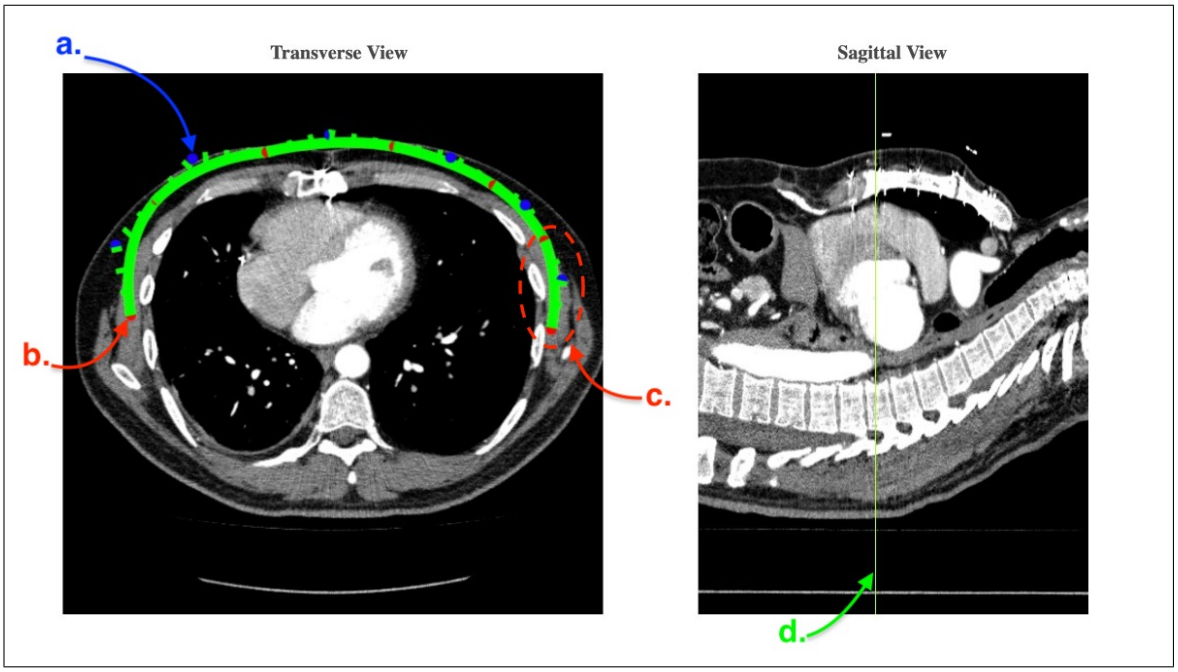

Figure 3.26 The curve drawing area of the GUI.

Finally, after the drawing and adjustments are made on final bar geometry, the start bending button is used to shape the bar. After clicking this button, a modal screen (in Figure 3.27) appears on the right side and prompts users to make some settings. If the user wants to make manual motor adjustment, he can control linear and rotational motors from the first compartment. The millimeter for the linear motor in the reserved region can be adjusted or tested manually by giving the input in degrees to the rotational motor. At the bottom, there are 2 input fields that must be filled before sending the information to the engine. The first one is the spring back angle. This angle varies according to the material used and the bending radius. Another information is the offset angle. Since the bar is not in direct contact with the bending head, there is a gap between them and the offset created by this gap must also be calculated. This information must also be provided since the offset depends on the bend distance. After providing the required input on the screen, pressing the start button starts the bending process wirelessly.

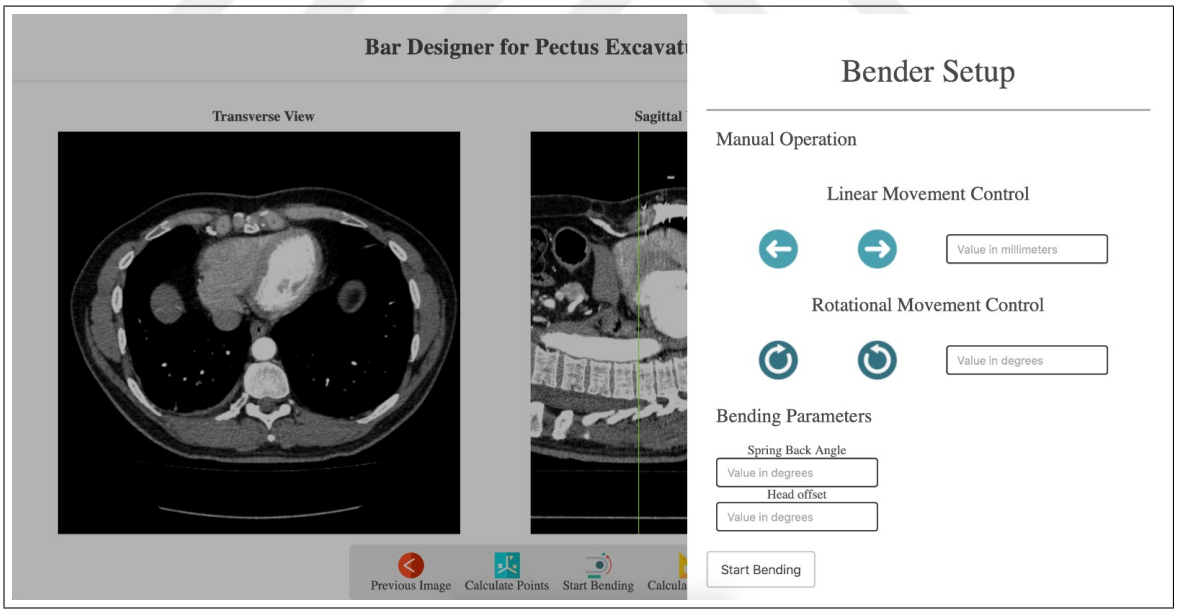

Figure 3.27 The bender setup screen of the GUI.

3.4.3 Embedded Software

3.4.3.1 Programming Language Selection. Embedded software inside the ESP8266 is the most crucial part of the bar bender and it retrieves data from Nodejs environment. Also, the software is capable of control the peripherals of the microcontroller in order to communicate with the bar bender machine. The whole process begins with the software starts to listen a predefined port on the server. As soon as the data is received from the designer, embedded software starts to convert data points into degrees. Since data points are sampled coordinates, it could be needed to extend or approximate the data. Although getting more samples is easy, the system requires more data points where the curvature angle is increased.If sampling rate is chosen according to only maximum curved point, the machine might do unnecessary computation and bending. For that reason, if bending sensitivity drops below 10mm, system automatically creates more sampling points since all control points are known, it is possible to create any combination of non-uniform sampling over the curve. This idea comes from mesh drawing process of 3D analysis software which aims decrease in computational time while keeping the accuracy level constant.

3.5 Bar Bending Process

The overview of the operation is shown on the x-y coordinates in Figure 3.28. Pectus bar bender machine is design to perform the bar bending starting from distal end. Therefore, the bar is fixed on one side and released on one side, in order not to go over the bended part again and to reduce the calculation and the complexity. Once the system is setup in that way, the only thing required is to calculate the angle between the specified bending points and the normal line. In this way, it is possible to make the bends on the normal line quickly. However, there are some potential problems at this point. The first of these problems was how to calculate the angles of the line. To solve this problem we have created a line representing the untwisted bar at the beginning of the curve. When this bar is bent from the end point to the head, if the bending point is small enough, any desired angle can be expressed as the sum of the smaller

angles. For example, if one wants a 100-degree angle with a 10mm radius and bends 10 degrees at 1mm intervals, the one reaches about 100 degrees in total, considering the calculation errors. Using this principle, we have reached the desired shape by bending the angle between the line and normal passing through each of the two bending points. Since the coordinates of all points are known, the cosine theorem is used to calculate this angle.

Another problem is at which points the line will pass with which slope. In order to solve this problem, the first two points on the curve are considered linear and it is assumed that they pass through a line. Since the first point is always offset to (0,0), the equation is a line with no constant term as y = mx. This is marked with the number 1 in the correct Figure 3.28 and is shown in light blue. Furthermore, the curves shown in Figure 3.28 numbered from 1 to 5 show the shape of the bar during bending, respectively.

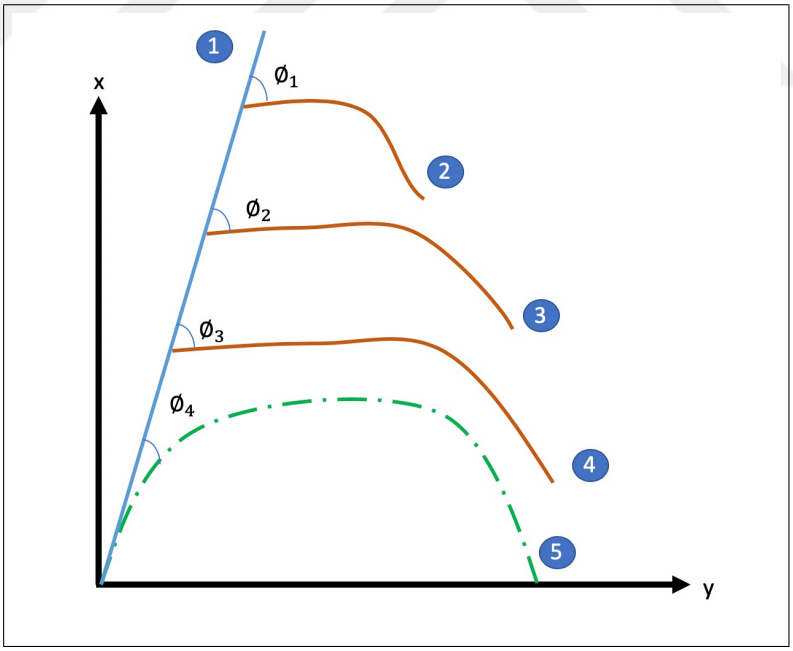

Figure 3.28 The process of bending: Points 1 through 5 shows the bending steps from a line to a curve.

Next the angle is converted to the motor steps by using pulse/revolution which is set to 360 steps.

4. RESULTS

4.1 Statement of Results

As a result, the images of the completed pectus bar bender prototype are given in Figure 4.1. The markings indicated in the figure are given in the following list.

1. The pectus bar.
2. Support point of twist.
3. Bending head.
4. Rear support point.
5. Rotational motion for motor drive.
6. Linear motion guide.
7. Belt mechanism.
8. Linear motion motor.
9. Transformer used in linear motor.

An image is also shown in Figure 4.2 during bending.

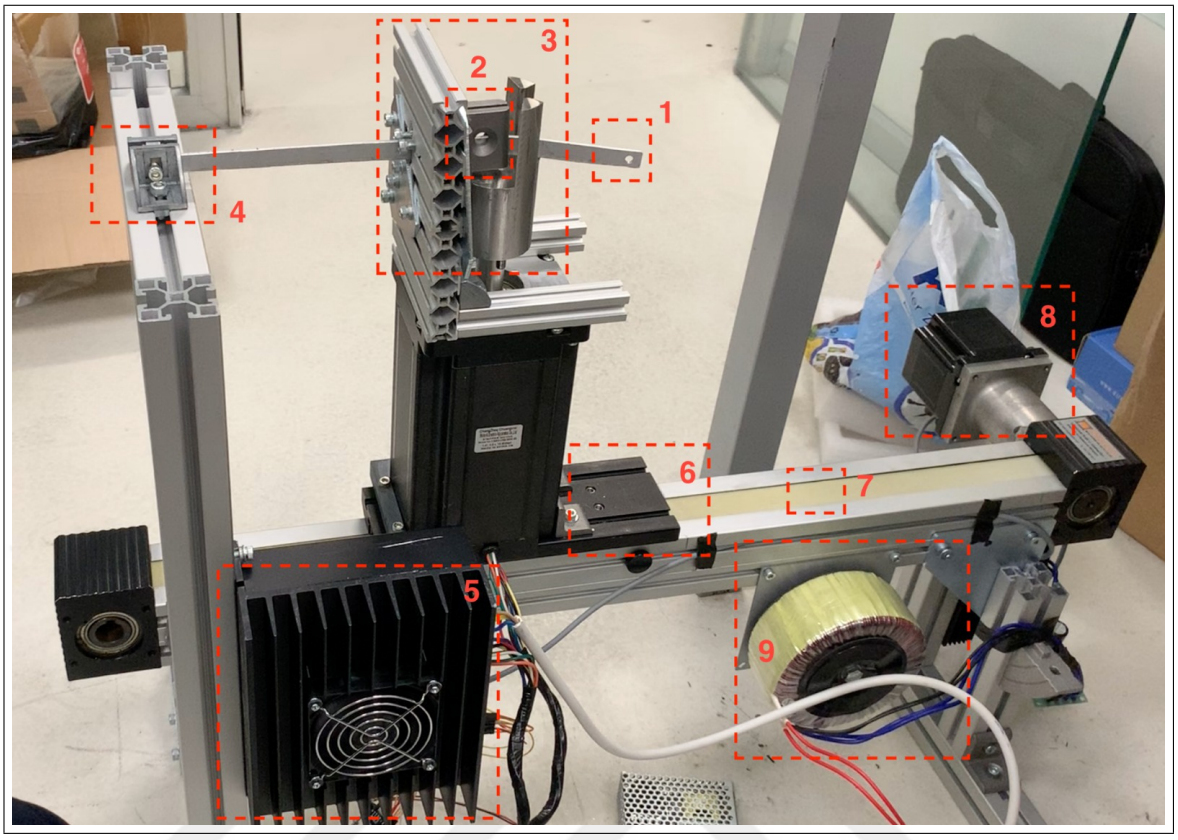

Figure 4.1 The final prototype of the designed system.

Figure 4.2 The real time bending procedure with designed system by GUI.

After the final prototype, completing several trials were conducted for the test. The measurement values for a plotted sample bar are given in Table 4.1. In this table, the first 2 columns of bar points drawn in pixels are given. In the third column, the angle calculation based on these values is given. The (x, y) coordinates in millimeters are the values measured after bending. The last column shows the error rate according to the actual value.

Table 4.1
Test results of bending procedure based on test sample.

Drawing Points		Calculated Angles in Degrees	Bent Bar Points		Error Rate in %
X coordinates in pixels	Y coordinates in pixels		X coordinates in [mm]	Y coordinates in [mm]	
7.44	12.98	0.00	5.47	9.56	N/A
18.33	23.25	16.84	13.91	18.29	3.01
31.60	30.16	39.80	23.25	22.20	0.03
46.03	34.10	58.65	33.83	25.08	0.14
60.90	35.81	71.79	44.83	26.36	0.02
76.62	36.37	78.83	56.38	26.77	0.02
91.60	35.68	85.72	67.42	26.26	0.01
105.94	31.39	101.12	77.96	23.11	0.02
119.49	23.17	119.15	87.23	17.05	5.93
128.30	11.85	136.26	94.47	8.71	0.04
135.47	-1.31	149.60	99.70	-1.00	0.01

The graph shown in Figure 4.3 is a comparison of the bent and drawn bar. As can be seen, there is a great similarity between the created bar and the drawn bar as expected. When the coordinate points are examined, all errors except 2 points are close to 0.

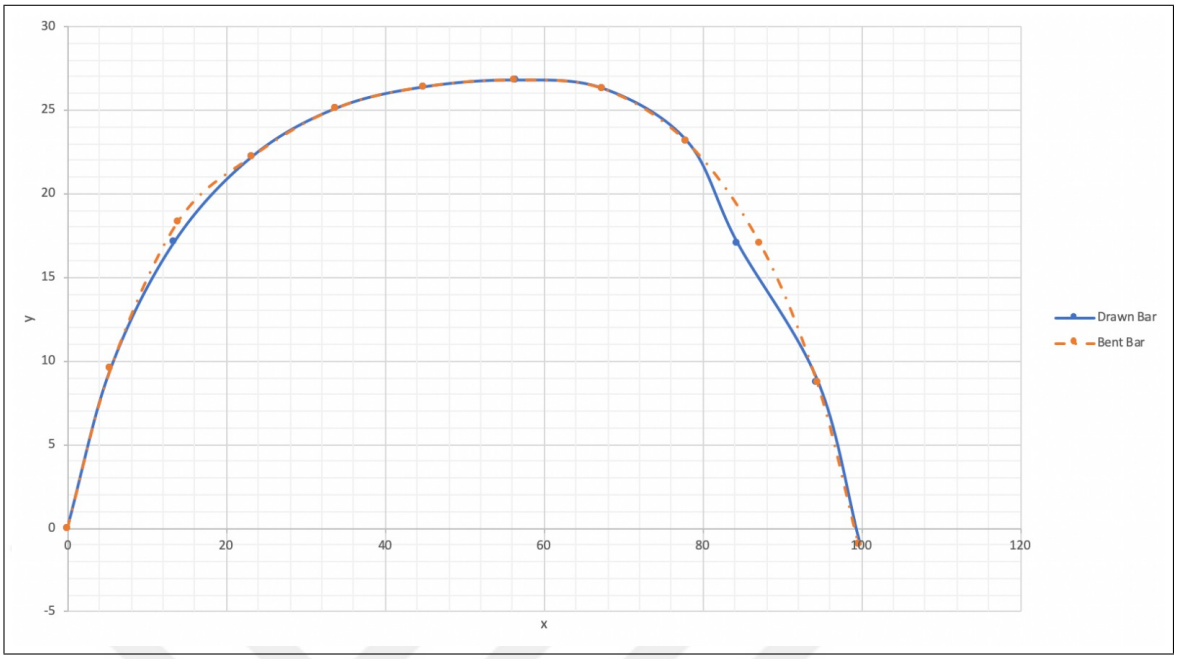

Figure 4.3 The graphs of drawn and bent bar coordinates.

The system was also tested the consultant surgeon for a sample based on real patient data. In this sample, the consultant surgeon determined the points where the bar would be placed on the saggital image and performed the bar drawing on the transverse image. The drawn and the shaped bar performed by the surgeon are given in Figure 4.4. The error in bar shaping as output is given in Table 4.2. The comparison plot between drawn bar and the bent bar is given in Figure 4.5. When this result is examined (in Table 4.2), it can be seen that some errors were occurred at the beginning of the bending process and then the cumulative error rate reed constant.

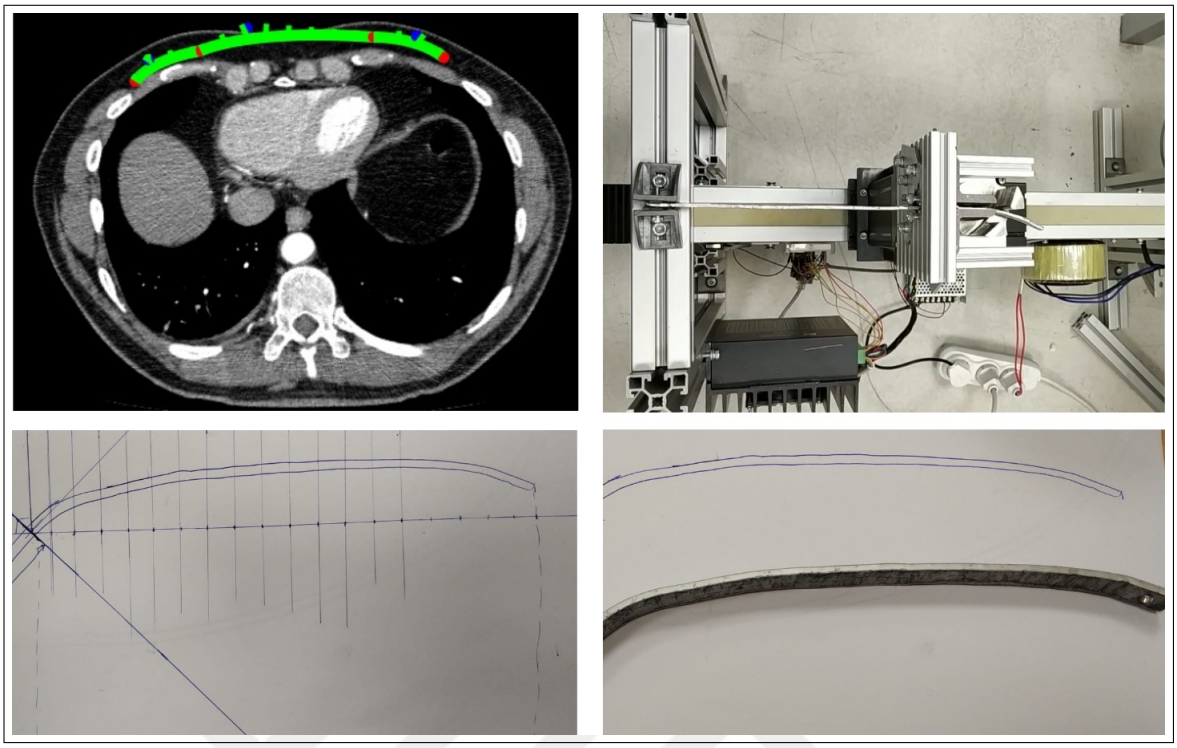

Figure 4.4 The bending procedure of bar drawn by the consultant surgeon.

Table 4.2
Test results of bending procedure based on real patient data.

Drawing Points		Calculated Angles in Degrees	Bent Bar Points		Error Rate in %
X coordinates in pixels	Y coordinates in pixels		X coordinates in [mm]	Y coordinates in [mm]	
10.57	0.63	6.57	6.87	0.70	N/A
23.79	17.70	17.38	17.51	12.40	4.82
37.95	22.55	28.82	27.93	15.80	4.79
52.51	25.98	39.35	38.65	18.70	2.21
67.01	30.75	48.52	49.32	20.80	8.11
81.42	34.91	65.50	59.93	23.80	7.36
96.19	37.69	71.88	70.80	26.30	5.19
111.04	39.50	74.30	81.72	27.80	4.38
126.02	40.61	76.43	92.75	28.30	5.32
141.12	41.17	78.31	103.87	28.70	5.28
156.25	41.28	80.04	115.00	29.00	4.54
171.20	41.02	81.64	126.00	28.20	6.60
186.18	40.47	83.23	137.03	28.80	3.31
201.28	39.65	90.50	148.14	28.00	4.05
216.55	39.04	93.40	159.38	26.60	7.42
231.45	37.95	106.28	170.35	25.70	8.00
246.12	34.82	119.79	181.14	23.90	6.74
260.01	29.31	125.92	191.37	20.60	4.49
272.66	21.27	132.54	200.68	15.10	3.52

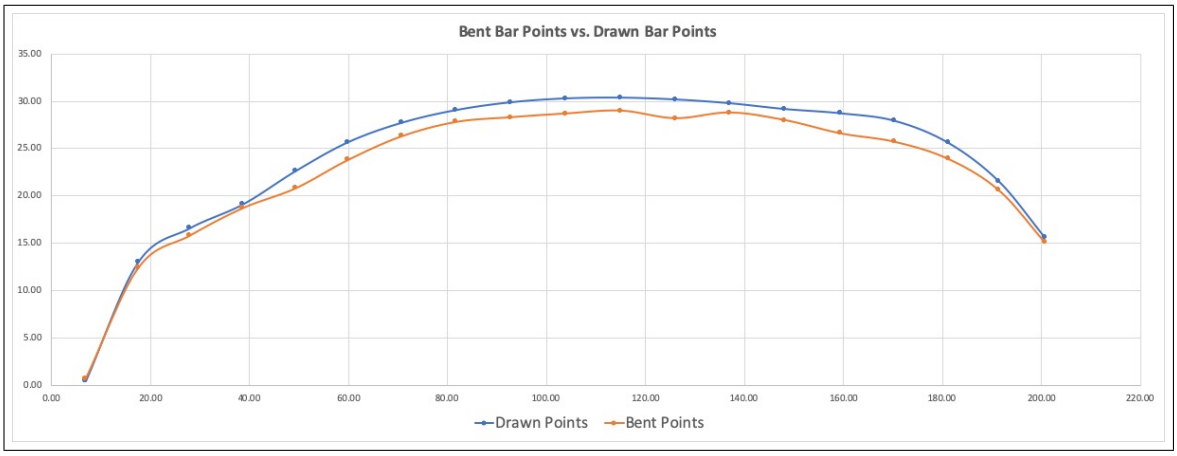

Figure 4.5 The graphs of drawn and bent bar coordinates.

5. CONCLUSION AND FUTURE WORKS

5.1 Conclusions

As a result, dedicated components software and hardware were completed at the prototype level. The system reads large image blocks quickly and distinguishes between metadata and slice display. Then sagittal image is created and displayed on the screen. The overall system was tested by a thoracic surgeon. The surgeon is able to design and form the bar shape before the operation. In addition, the simple interface makes measurements and bar creation simple and fast. The consultant surgeon provided positive feedback. He stated that the system can primarily guide surgeons with moderate experience, and provide experienced surgeons the opportunity to be more prepared in advance. In addition, he commented that the system's speed and low error would facilitate operations.

When the sensitivity, shape and error rates of the previously bent bars were examined, it was also confirmed by the surgeon the system was operating adequately. In the first bent sample bar, more than 1% error was made at 2 points, although the first and last points were correctly positioned. In this example, the highest error is around 5%. Since the system hardware cannot detect the error yet, a constant rate of error continues even if all the points are bent correctly from the point where the error occurred. An example of this is shown in the bar bent given in Table 4.2. An initial error of about 5% was followed along all points. Furthermore, in this example, the reason for the errors being distributed differently is that the bar has been bent several times previously and causing the form distortions on the bar.

5.2 Statement of Existing Problems

There are differences in the system than originally planned. In particular, we had to modify our original design due to expensive third party components, and the manufacturers' refusal to manufacture for custom parts. In the first stage, instead of some planned parts, lower quality parts that could be equivalent were preferred such as the bend support. The support part and the lower support points of the motor which were initially intended to be manufactured from a steel block using CNC. Some parts were manufactured using PTFE, thermopolymer. These components perform their function at a high rate by taking advantage of less load on the lower parts of the motor. However, due to the low solubility in production, the parts could not be mounted tightly to the motor. Therefore, the electric motor initially moves slightly due to the effect of torque and vibration, which increases the error rate. This effect is not continuous as the weight of the electric motor damps a continuous movement and vibration.

Another part, the upper support, could not be produced for similar reasons as the lower retaining parts. This part was replaced by a combination of 2 aluminum profiles 20x60x100mm in size and the joining pieces used in sigma profiles. A hole was drilled on the aluminum profile so that the bar could find an area to move. The biggest problem with this part is that it does not fully transfer the stress on the motor body during bending. Therefore, flexes occur due to the high torques generated on the support part. These flexures also adversely affect the twist resolution.

One of the major problems is that the bending motor does not reach the required power. Even in the high torque class, which is rarely available on the market, even this stepper motor is not entirely sufficient to bend the steel alloy. Although the motor began to bend steel, it was never possible to achieve an accurate result because of frequent tooth jumps.

5.3 Limitations

The project is successful in automated pectus bar bending and has some limitations based on desired geometry created by the software. As far as the bending angle is concerned, the support point is positioned close to the motor center to increase torque and cannot make 360-degree rotations due to the fork-shaped bending head geometry. In fact, the maximum angle of rotation is measured as 85 degrees. Since some of this angle is used as offset and spring back angle, there is a margin of approximately 50 degrees. However, since the system is based on the principle of cumulative growth of angles, this problem can be overcome by increasing the resolution of the movement along the x-axis. The limit values are given in Table 5.1.

Table 5.1
Limit values of the manufactured prototype.

	Limit Values
Max current bender motor	3.6 A
Max torque of bender motor	28 Nm
Max bend turn angle of bender motor	85 degrees
Maximum bar length	100 cm
Minimum bar length	10 cm
Minimum offset of bender head	20 degrees
Maximum effective bending degree	65 degrees

Another limitation relates to movement on the minimum x-axis. In fact, the system offers a motion resolution of less than 1 millimeter, but the actual amount required to move must be the difference between the support point and the bending point so that the system can consistently bend over 2 linear points. If a bend is attempted between a linear point and a non-linear point, a process load, such as calculating how far the previous point will proceed, may be encountered.

The final limitation is the measurement of dead points that cannot be bent on a bar. These points are actually the length required to prevent the retention point from colliding with the support point. This length is approximately 10cm in the current system. However, this limitation can be overcome by design of the holding point so that it can pass through the support area. In order to realize the redesigning, a stronger

material such as steel should be used instead of aluminum.

5.4 Future Works

The system is designed to be improved by building tenance. The first aim is to increase the production quality of materials and custom parts and accuracy. Subsequent replacement of the stepper motor with the more expensive servo motor, where special improvements can be made, can help to improve the production quality. A servo motor with twice the torque can replace existing motor.

The linear drive is very successful and has been chosen to withstand more torque. However, there is a trade off between weight and rigidity in the material selection of the bending mechanism. If the materials are to be purchased at an acceptable price range, the weight will increase, as it will have to be directed to high strength and high-density materials such as steel. To prevent this, instead of solid steel blocks, blocks of hollow structures with high strength will be designed in the future. In addition, it is aimed to increase the support during twisting with 2 worm shafts which will move with the motor to reduce the tension on the upper side. Finally, it is aimed to create and share the software as an open source project on the software side and develop an algorithm that can store patient information safely and enable DICOM files to be processed more efficiently.

REFERENCES

1. Abid, I., M. M. Ewais, J. Marranca, and D. E. Jaroszewski, "Pectus excavatum: a review of diagnosis and current treatment options," *J Am Osteopath Assoc*, Vol. 117, no. 2, pp. 106–113, 2017.

2. Haecker, F.-M., and S. Sesia, "Non-surgical treatment of pectus excavatum," *Journal of Visualized Surgery*, Vol. 2, 2016.

3. Microfixation, B., *Pectus Excavatum Correction*. Biomet Microfixation, Jacksonville, FL, 2013. r45k1003.

4. Pocock, G., C. D. Richards, and D. A. Richards, *Human Physiology*, Oxford University Press, 2013.

5. Salam, H., *Pectus Excavatum - Radiology Case - Radiopaedia.org*, 2010. (rID:8657).

6. Sherwood, L., *Human Physiology: From Cells to Systems*, Cengage learning, 2015.

7. Kutluk, A. C., and M. Metin, "Congenital chest wall deformities," *The Journal of Turkish Spinal Surgery*, Vol. 28, no. 3, pp. 195–204, 2017.

8. Bryant, A., R. Cerfolio, D. Sugarbaker, R. Bueno, M. Krasna, S. Mentzer, and L. Zellos, "Adult chest surgery," 2009.

9. Kuhn, M. A., and D. Nuss, "Pectus deformities," in *Fundamentals of Pediatric Surgery*, pp. 313–321, Springer, 2011.

10. Huddleston, C. B., "Pectus excavatum," in *Seminars in Thoracic and Cardiovascular Surgery*, Vol. 16, pp. 225–232, Elsevier, 2004.

11. Chin, E., and R. H. Adler, "The surgical treatment of pectus excavatum (funnel chest)," *British Medical Journal*, Vol. 1, no. 4870, p. 1064, 1954.

12. Lester, C. W., "The etiology and pathogenesis of funnel chest, pigeon breast, and related deformities of the anterior chest wall.," *The Journal of Thoracic Surgery*, Vol. 34, no. 1, p. 1, 1957.

13. Cook, R., "Observations on the etiology of pectus excavatum and other chest deformities, and the method of recording them: K. mullard. brit. j. surg. 54:(no. 2): 115–120, feb. 1967," *Journal of Pediatric Surgery*, Vol. 2, no. 6, p. 594, 1967.

14. Hecker, W., G. Procher, and H. Dietz, "Results of operative correction of pigeon and funnel chest following a modified procedure of ravitch and haller (author's transl)," *Zeitschrift fur Kinderchirurgie: Organ der Deutschen, der Schweizerischen und der Osterreichischen Gesellschaft fur Kinderchirurgie= Surgery in infancy and childhood*, Vol. 34, no. 3, pp. 220–227, 1981.

15. Kelly Jr, R. E., M. L. Lawson, C. N. Paidas, and R. H. Hruban, "Pectus excavatum in a 112-year autopsy series: anatomic findings and the effect on survival," *Journal of Pediatric Surgery*, Vol. 40, no. 8, pp. 1275–1278, 2005.

16. Serafin, J., J. Swiatkowski, R. Majkusiak, and P. Nowakowski, "40-year experience in surgical treatment of congenital chest deformations–ethiopathogenesis, operative techniques and clinical results.," *Acta Chirurgiae Orthopaedicae et Traumatologiae Cechoslovaca*, Vol. 70, no. 4, pp. 207–213, 2003.

17. Shamberger, R., and K. Welch, "Cardiopulmonary function in pectus excavatum.," *Surgery, gynecology & obstetrics*, Vol. 166, no. 4, pp. 383–391, 1988.

18. Gurnett, C. A., F. Alaee, A. Bowcock, L. Kruse, L. G. Lenke, K. H. Bridwell, T. Kuklo, S. J. Luhmann, and M. B. Dobbs, "Genetic linkage localizes an adolescent idiopathic scoliosis and pectus excavatum gene to the 18q chromosome," *Spine*, Vol. 34, no. 2, p. E94, 2009.

19. Ravitch, M. M., *Congenital Deformities of the Chest Wall and Their Operative Correction*, WB Saunders Company, 1977.

20. Coulson, W., *On Deformities of the Chest*, Hurst, 1836.

21. Saxena, A. K., "History of surgical repairs of chest wall deformities," in *Chest Wall Deformities*, pp. 3–18, Springer, 2017.

22. Lane-Smith, D., D. Gillis, and P. Roy, "Repair of pectus excavatum using a dacron vascular graft strut," *Journal of Pediatric Surgery*, Vol. 29, no. 9, pp. 1179–1182, 1994.

23. Rehbein, F. v., and H.-H. Wernicke, "The operative treatment of the funnel chest," *Archives of Disease in Childhood*, Vol. 32, no. 161, p. 5, 1957.

24. Ochsner, A., "Chone-chondrosternon: report of a case and review of the literature," *J Thorac Surg*, Vol. 8, pp. 469–511, 1939.

25. Nissen, R., "Osteoplastic procedure for correction of funnel chest," *The American Journal of Surgery*, Vol. 64, no. 2, pp. 169–174, 1944.

26. Ravitch, M. M., "The operative treatment of pectus excavatum," *Annals of surgery*, Vol. 129, no. 4, p. 429, 1949.

27. Wallgren, G., and M. Sulamaa, "Surgical treatment of funnel chest. exhib. viii," *International Congress Pediatric. p32*, 1956.

28. Adkins, P., and B. Blades, "A stainless steel strut for correction of pectus escavatum.," *Surgery, Gynecology & Obstetrics*, Vol. 113, p. 111, 1961.

29. Welch, K. J., and G. P. Kearney, "Abdominal musculature deficiency syndrome: prune belly," *The Journal of Urology*, Vol. 111, no. 5, pp. 693–700, 1974.

30. Welch, K., and R. Shamberger, "Chest wall deformities," *General Thoracic Surgery*, Vol. 3, 1980.

31. Nuss, D., R. E. Kelly Jr, D. P. Croitoru, and M. E. Katz, "A 10-year review of a minimally invasive technique for the correction of pectus excavatum," *Journal of Pediatric Surgery*, Vol. 33, no. 4, pp. 545–552, 1998.

32. Scherer, L., P. H. Arn, D. A. Dressel, R. M. Pyeritz, and J. A. Haller Jr, "Surgical management of children and young adults with marfan syndrome and pectus excavatum," *Journal of Pediatric Surgery*, Vol. 23, no. 12, pp. 1169–1172, 1988.

33. Waters, P., K. Welch, L. J. Micheli, R. Shamberger, and J. E. Hall, "Scoliosis in children with pectus excavatum and pectus carinatum.," *Journal of Pediatric Orthopedics*, Vol. 9, no. 5, pp. 551–556, 1989.

34. Saxena, A., and G. Willital, "Surgical correction of funnel chest using titanium struts," *Surg Childh Intern*, Vol. 6, pp. 230–2, 1998.

35. Osawa, H., T. Mawatari, A. Watanabe, and T. Abe, "New material for nuss procedure," *Ann Thorac Cardiovasc Surg*, Vol. 10, no. 5, pp. 301–3, 2004.

36. Robicsek, F., "Surgical treatment of pectus excavatum.," *Chest Surgery Clinics of North America*, Vol. 10, no. 2, pp. 277–296, 2000.

37. Croitoru, D. P., R. E. Kelly Jr, M. J. Goretsky, M. L. Lawson, B. Swoveland, and D. Nuss, "Experience and modification update for the minimally invasive nuss technique for pectus excavatum repair in 303 patients," *Journal of Pediatric Surgery*, Vol. 37, no. 3, pp. 437–445, 2002.

38. Schaarschmidt, K., A. Kolberg-Schwerdt, M. Lempe, F. Schlesinger, K. Bunke, and J. Strauss, "Extrapleural, submuscular bars placed by bilateral thoracoscopy- a new improvement in modified nuss funnel chest repair," *Journal of Pediatric Surgery*, Vol. 40, no. 9, pp. 1407–1410, 2005.

39. Schier, F., M. Bahr, and E. Klobe, "The vacuum chest wall lifter: an innovative, nonsurgical addition to the management of pectus excavatum," *Journal of Pediatric Surgery*, Vol. 40, no. 3, pp. 496–500, 2005.

40. Futagawa, K., I. Suwa, T. Okuda, H. Kamamoto, J. Sugiura, R. Kajikawa, and Y. Koga, "Anesthetic management for the minimally invasive nuss procedure in 21 patients with pectus excavatum," *Journal of Anesthesia*, Vol. 20, no. 1, pp. 48–50, 2006.

41. Nuss, D., and R. E. Kelly, "Minimally invasive surgical correction of chest wall deformities in children (nuss procedure)," *Advances in Pediatrics*, Vol. 55, no. 1, pp. 395–410, 2008.

42. Türk, F., G. Yuncu, and E. Türk, "Konjenital göğüs deformitelerinde tarihsel süreç," *Journal of Clinical and Analytical Medicine*, pp. 52–57, 2010.

43. Şahin, A., "Pektus ekskavatumun açık operasyonla düzeltilmesi," *Turkiye Klinikleri Thoracic Surgery-Special Topics*, Vol. 9, no. 1, pp. 67–71, 2018.

44. Kılıç, B., and M. K. Kaynak, "Pektus ekskavatumda minimal invaziv teknik," *Turkiye Klinikleri Thoracic Surgery-Special Topics*, Vol. 9, no. 1, pp. 72–74, 2018.

45. Kelly Jr, R. E., R. C. Shamberger, R. B. Mellins, K. K. Mitchell, M. L. Lawson, K. Oldham, R. G. Azizkhan, A. V. Hebra, D. Nuss, M. J. Goretsky, *et al.*, "Prospective multicenter study of surgical correction of pectus excavatum: design, perioperative complications, pain, and baseline pulmonary function facilitated by internet-based data collection," *Journal of the American College of Surgeons*, Vol. 205, no. 2, pp. 205–216, 2007.

46. Shamberger, R. C., and K. J. Welch, "Surgical repair of pectus excavatum," *Journal of Pediatric Surgery*, Vol. 23, no. 7, pp. 615–622, 1988.

47. Guller, B., and K. Hable, "Cardiac findings in pectus excavatum in children: review and differential diagnosis," *Chest*, Vol. 66, no. 2, pp. 165–171, 1974.

48. Key, T., *Fastest Thoracic Insight Engine.* Available: https://thoracickey.com/indexes-for-pectus-deformities/, last accessed on 03/11/19.

49. Kolvekar, S., and H. Pilegaard, *Chest wall Deformities and Corrective Procedures*, Springer, 2016.

50. Cartoski, M. J., D. Nuss, M. J. Goretsky, V. K. Proud, D. P. Croitoru, T. Gustin, K. Mitchell, E. Vasser, and R. E. Kelly Jr, "Classification of the dysmorphology of pectus excavatum," *Journal of Pediatric Surgery*, Vol. 41, no. 9, pp. 1573–1581, 2006.

51. Yoshida, A., S. Uemura, M. Yamamoto, H. Nouso, H. Kuyama, and Y. Muta, "Correlation of asymmetric chest wall deformity and growth in patients with pectus excavatum," *Journal of Pediatric Surgery*, Vol. 48, no. 4, pp. 771–775, 2013.

52. Yüksel, M., and A. A. Balcı, *Göğüs Cerrahisi:" Kırmızı Kitap"*, Nobel Tıp Kitabevi, 2015.

53. Sesia, S. B., F.-M. Haecker, B. Shah, M. J. Goretsky, R. E. Kelly Jr, and R. J. Obermeyer, "Development of metal allergy after nuss procedure for repair of pectus excavatum despite preoperative negative skin test," *Journal of Pediatric Surgery Case Reports*, Vol. 1, no. 6, pp. 152–155, 2013.

54. Pianykh, O. S., *Digital imaging and communications in medicine (DICOM): a practical introduction and survival guide*, Springer Science & Business Media, 2009.

55. Yock, P. G., T. M. Krummel, and C. Kurihara, *Biodesign*, Cambridge University Press, 2015.

56. Elias, A. A., R. Y. Cavana, and L. S. Jackson, "Stakeholder analysis for r&d project management," *R&D Management*, Vol. 32, no. 4, pp. 301–310, 2002.

57. Technology, L., *STEPPING MOTORS Type 110BHH199-560E-55*. Leadshine Technology, China, 2013. REV. 1.0.

58. Espressif Inc., SHANGHAI, *ESP8266EX Datasheet*, 2019. Version 6.2.

59. Espressif Inc., SHANGHAI, *ESP8266 Hardware Design Guidelines*, 2019. Version 2.6.

60. Kalip, D., *64x64 Lineer Triger Kompakt Modül*. Dogus Kalip, Turkey. Available: https://www.doguskalip.com.tr/Urun/64x64-lineer-triger-kompakt-modul/1289, last accessed on 08/10/19.

61. Changzhou Chuangwei Motor & Electric Apparatus Co., L., *Stepper Motor Driver CW2283*. Changzhou Chuangwei Motor & Electric Apparatus Co., Ltd., China, 2013. REV. 1.0.

62. Changzhou Chuangwei Motor & Electric Apparatus Co., L., *Digital Stepper Driver CW556-A*. Changzhou Chuangwei Motor & Electric Apparatus Co., Ltd., China, 2015. REV. 1.0.

63. *A brief history of Node.js*, 2019. Available: https://nodejs.dev/a-brief-history-of-nodejs, last accessed on 15/11/19.

64. Association, N. E. M., "Digital Imaging and Communications in Medicine (DICOM) Standard," NEMA PS3 / ISO 12052, Rosslyn, VA, USA.

65. Federle, M. P., M. L. Rosado-de Christenson, S. P. Raman, B. W. Carter, P. J. Woodward, and A. M. Shaaban, *Imaging Anatomy: Chest, Abdomen, Pelvis E-Book*, Elsevier Health Sciences, 2016.

66. Biswas, S., and B. C. Lovell, *Bézier and Splines in Image Processing and Machine Vision*, Springer Science & Business Media, 2007.

67. Association, N. E. M., "Digital Imaging and Communications in Medicine (DICOM) Standard - Pixel Spacing Attribute - X-Ray Acquisition Module," NEMA PS3.3 2019e, Rosslyn, VA, USA.